NEUROSCIENCE

Syntaxin 1 Ser^{14} phosphorylation is required for nonvesicular dopamine release

Aparna Shekar[1]†, Samuel J. Mabry[1]†, Mary H. Cheng[2]†, Jenny I. Aguilar[1], Shalin Patel[1], Daniele Zanella[1], David P. Saleeby[1], Yanqi Zhu[1], Tiziana Romanazzi[3], Paula Ulery-Reynolds[4], Ivet Bahar[2]‡, Angela M. Carter[1]‡, Heinrich J. G. Matthies[1]‡, Aurelio Galli[1]‡*

Amphetamine (AMPH) is a psychostimulant that is commonly abused. The stimulant properties of AMPH are associated with its ability to increase dopamine (DA) neurotransmission. This increase is promoted by nonvesicular DA release mediated by reversal of DA transporter (DAT) function. Syntaxin 1 (Stx1) is a SNARE protein that is phosphorylated at Ser^{14} by casein kinase II. We show that Stx1 phosphorylation is critical for AMPH-induced nonvesicular DA release and, in *Drosophila melanogaster*, regulates the expression of AMPH-induced preference and sexual motivation. Our molecular dynamics simulations of the DAT/Stx1 complex demonstrate that phosphorylation of these proteins is pivotal for DAT to dwell in a DA releasing state. This state is characterized by the breakdown of two key salt bridges within the DAT intracellular gate, causing the opening and hydration of the DAT intracellular vestibule, allowing DA to bind from the cytosol, a mechanism that we hypothesize underlies nonvesicular DA release.

INTRODUCTION

Amphetamine (AMPH) is a psychostimulant commonly used clinically to treat neuropsychiatric disorders, most notably, attention deficit disorders (*1*). There are estimated to be 56 million AMPH users worldwide (*2*). In 2020, the Substance Abuse and Mental Health Services Administration reported that about 2.6 million people in the United States have used AMPHs in the past year, while approximately 1.5 million have AMPH use disorders, underscoring its abuse potential. Since 2008, hospitalizations related to AMPH and its derivatives (e.g., methamphetamine) have increased to a greater degree than those associated with other abused substances (*3*). Furthermore, in 2015, annual hospital costs associated with abuse of AMPHs were $2.17 billion, highlighting the public health impact and the societal cost of these drugs (*3*), as well as the need to uncover new pharmacological targets for the treatment of AMPH abuse.

The abuse potential and psychomotor stimulant properties of AMPHs have been associated with their ability to cause mobilization of cytoplasmic dopamine (DA), leading to an increase in extracellular (EC) DA levels (*4*–*6*). This increase is mediated by nonvesicular DA release (DA efflux), which is the result of reversal of the DA transporter (DAT) (*4*), promoted by AMPH. The physiological function of DAT is to shape central DA neurotransmission via reuptake of synaptically released DA (*7*). Notably, inhibition of DA efflux reduces both the ability of AMPH to increase motor activity and AMPH preference (*8*–*11*). Thus, identifying the molecular underpinnings of AMPH-induced DA efflux, understanding how they affect DA neurotransmission, and translating these events to specific behavioral phenotypes associated with AMPH exposure are pivotal steps for providing new therapeutic targets for AMPH abuse.

AMPH is a substrate for DAT and is transported across the plasma membrane in a Na^+-dependent manner, similar to DA (*4*, *12*, *13*). Uptake of a substrate through DAT is determined by five conformation states that the transporter adopts: outward-open (O_o), outward-occluded, holo-occluded (H_{occ}), inward-occluded, and inward-open (I_o) (*14*, *15*). In the O_o state, the binding pocket is accessible to water and substrate, as well as sodium and chloride ions that bind in the immediate vicinity of the substrate (*14*). DA, along with its cotransported ions, binds to DAT in the O_o conformation. This binding induces a shift through the occluded states as intermediates. Molecular dynamics (MD) simulations have garnered additional insight into the mechanism of DA transport. Notably, it was found that in the H_{occ} state, both the EC and intracellular (IC) gates are closed, and both the EC and IC vestibules are inaccessible to water (*15*). In this conformation, there is the formation of a salt bridge, E428-K260, and the breaking of E428-R445 and K66-D345 salt bridges that control the IC vestibule gate (*15*). This shift allows the transporter to begin the transition to the I_o state (*15*). Once it reaches the I_o state, DA and its cotransported ions are released into the cytosol.

In addition to inducing DA efflux (*4*, *5*, *16*–*18*), AMPH also stimulates calcium/calmodulin-dependent protein kinase II (CAMKII) and protein kinase C, which, in turn, phosphorylate the DAT N terminus (*19*–*23*). This phosphorylation is required for DA efflux (*18*, *21*, *22*). There are five main phosphorylation sites at the distal N terminus, which include Ser2, Ser4, Ser7, Ser12, and Ser13 (*24*). Deletion of the 22 most distal amino acids or substitution of these Ser to Ala does not alter DAT surface expression, surface localization, or DAT-mediated DA uptake, while it does impair AMPH-induced DA efflux (*18*, *24*, *25*). However, how phosphorylation of the DAT N terminus promotes DA efflux and the molecular players involved in this process are still largely unknown.

[1]Department of Surgery, University of Alabama at Birmingham, Birmingham, AL, USA. [2]Department of Computational and Systems Biology, University of Pittsburgh School of Medicine, Pittsburgh, PA, USA. [3]Department of Biotechnology and Life Sciences, University of Insubria, Varese, Italy. [4]Department of Psychiatry, UT Southwestern Medical Center, Dallas, TX, USA.
†These authors contributed equally to this work.
‡These authors contributed equally to this work.
*Corresponding author. Email: agalli@uabmc.edu

Syntaxin 1 (Stx1) is a soluble *N*-ethylmaleimide–sensitive factor attachment protein receptor (SNARE) protein that plays a key role in vesicular synaptic release (*26*) and is regulated by Munc18-1 binding (*27*, *28*). In addition to its role in vesicular fusion, Stx1 interacts with and regulates the function of transmembrane proteins, including ion channels and transporters (*10*, *29*–*33*). Stx1 directly interacts with the DAT N terminus within the first 33 amino acids (*30*). This DAT domain includes the five most distal Ser, whose phosphorylation is involved in DA efflux (*16*, *18*). AMPH promotes DAT-Stx1 association, as well as Stx1 phosphorylation at Ser^{14} (*10*, *30*). This association occurs at the plasma membrane (*30*) and is regulated by Stx1 phosphorylation, an event mediated by casein kinase 2 (CK2) (*10*, *34*). In addition to regulating AMPH actions (*10*), the pivotal role played by Stx1 phosphorylation in neuropsychiatric disorders associated with DA dysfunction is underscored by the involvement of CK2 impairments in the etiology of both autism and schizophrenia (*35*).

In this study, we delineate the temporal dynamics of AMPH-induced Stx1 phosphorylation and the role played by this phosphorylation on nonvesicular DA release and its associated behaviors. Furthermore, to understand the molecular mechanisms of how Stx1 phosphorylation promotes AMPH-induced DAT-mediated DA efflux, we performed MD simulations of the DAT/Stx1 complex. Our results support a model where AMPH, by coordinating DAT N terminus and Stx1 phosphorylation, causes DAT to form an aqueous channel–like pore where DA molecules bind the DAT IC vestibule from the cytoplasm and, thereby, cross the plasma membrane to support DA efflux.

RESULTS

AMPH promotes Stx1 phosphorylation and reorganizes the hDAT/Stx1 complex

AMPH induces CK2-mediated Stx1 phosphorylation at S14 (pS14) (*10*) and binding of Stx1 to the DAT N terminus (*10*, *30*, *36*). These events are vital for the ability of AMPH to cause DA efflux and associated behaviors (*10*, *30*). We defined the temporal dynamics of AMPH-induced Stx1 phosphorylation, the key players implicated, and the structural domains involved in DAT-Stx1 interactions. In human DAT (hDAT) cells (see Materials and Methods), AMPH treatment causes a significant increase in pS14 at 5, 10, and 15 min. However, after 30 min of AMPH exposure, the level of Stx1 phosphorylation was not significantly different compared to baseline (Fig. 1A). This normalization in the levels of Stx1 pS14 is possibly due to the ability of AMPH to increase IC Ca^{2+} (*37*), shown to activate the protein phosphatases type 1 family (*38*). This family of phosphatases targets Stx1 at the S14 site (*39*).

To further explore this AMPH-induced phosphorylation event, we focused on CK2, a kinase implicated in Stx1 pS14 (*10*, *34*). We treated hDAT cells with the CK2 inhibitor (CK2i), CX-4945 (*40*), before (6 hours) and during AMPH exposure. We found that CK2i blocks Stx1 phosphorylation in response to AMPH treatment (Fig. 1B). Consistent with this CK2 activity, docking simulations between CK2 and Stx1 support a model where CK2 is capable of phosphorylating Stx1 at S14 (fig. S1A), i.e., Stx1 S14 makes close contact with the CK2 catalytic residue, D156. However, CK2i does not significantly reduce basal Stx1 phosphorylation (Fig. 1B, inset). These data demonstrate that CK2 mediates AMPH-induced Stx1 phosphorylation, that this phosphorylation is time-dependent, and that it peaks shortly after AMPH administration. They also suggest that under basal conditions, CK2 is limited in determining the level of Stx1 pS14.

Considering that the AMPH-induced hDAT-Stx1 interaction regulates DA efflux (*30*) and behaviors (*10*), we next defined the temporal dynamics of AMPH-induced hDAT-Stx1 associations. hDAT cells were exposed to AMPH for different time periods, and then hDAT was immunoprecipitated. The immunoprecipitates were then immunoblotted for Stx1 (Fig. 1C, top). The interaction between hDAT and Stx1 peaked at 5 min of AMPH exposure (Fig. 1C, bottom), a time that closely corresponds to maximum Stx1 phosphorylation (Fig. 1A). Thus, it is possible that the interactions between hDAT and Stx1 are tightly regulated by Stx1 phosphorylation status. Consistent with this hypothesis, this interaction returned to baseline by 40 min (Fig. 1C, bottom), similar to what was observed for Stx1 phosphorylation (Fig. 1A).

The question remains of how Stx1 pS14 regulates the structural interactions between hDAT and Stx1. First, we generated structural models for the complex of hDAT wild type (WT) with Stx1 WT using full-length hDAT in an occluded conformation (*41*) and the Stx1 structure modeled by Robetta (*42*), using ClusPro (*43*). Then, we performed MD simulations of the hDAT-Stx1 complex in the presence or absence of a phospho group at Stx1 S14 (Stx1 pS14). In Fig. 1D, we show the resulting complex formed by hDAT and Stx1 embedded in a membrane (*44*) with surrounding water molecules, ions, and lipids, including phosphatidylinositol 4,5-bisphosphate (PIP_2), obtained after 10-ns MD simulations. In this complex, the interfacial interactions between hDAT and Stx1 involve multiple salt bridges: Stx1 D15/D17 and hDAT R344, Stx1 R26 and hDAT E56, and Stx1 E38/E39 and hDAT R51 [Fig. 1, D (inset) and E (100-ns snapshot)]. Notably, mutations associated with autism (R26Q in Stx1 and R51W in hDAT), which would result in disruption of these predicted salt bridges, have been implicated in altering hDAT-Stx1 interactions, Stx1 phosphorylation, and DA efflux (*10*). The N-terminal segment of Stx1 (M1-R26) is highly charged, carrying four positive and eight negative charges. Five contiguous acidic residues (D15 to D19) form a negative cluster in proximity to S14. In contrast, the cytoplasmic side of hDAT contains a cluster of basic residues that attract the acidic portions of Stx1. In particular, the basic cluster in hDAT containing R344 and K65/K66 is predicted to be near the D15 to D19 Stx1 acidic cluster (Fig. 1D, inset).

We also found that PIP_2 coordinates some of the hDAT WT-Stx1 interactions. In our MD simulations, we consistently observed two to four PIP_2 molecules binding to the interface between hDAT WT (R515, R521, and K525) and the N terminus of Stx1 (K2, R4, and R9) (circled in Fig. 1F), which is consistent with the observation that Stx1 N terminus interacts with PIP_2 (*45*). The hDAT WT/Stx1 complex includes two additional PIP_2 binding sites: one (Fig. 1F, cyan licorice) is near K65/K66 of DAT and R26/R28 of Stx1 and the other (Fig. 1F, purple licorice) is near K3/K5 and R443 of DAT. Consistent with this model, we previously identified a basic cluster (including K3 and K5) at the N terminus and the fourth IC loop (IL4; R443) as PIP_2 binding sites (*8*, *9*). In the MD simulations of the complex between hDAT WT and Stx1 pS14, the pS14 destabilized the S14 to D19 segment of Stx1 and triggered its dissociation from hDAT WT K65/K66 and R344 (Fig. 1G, snapshot at 100 ns, and fig. S1, B to D).

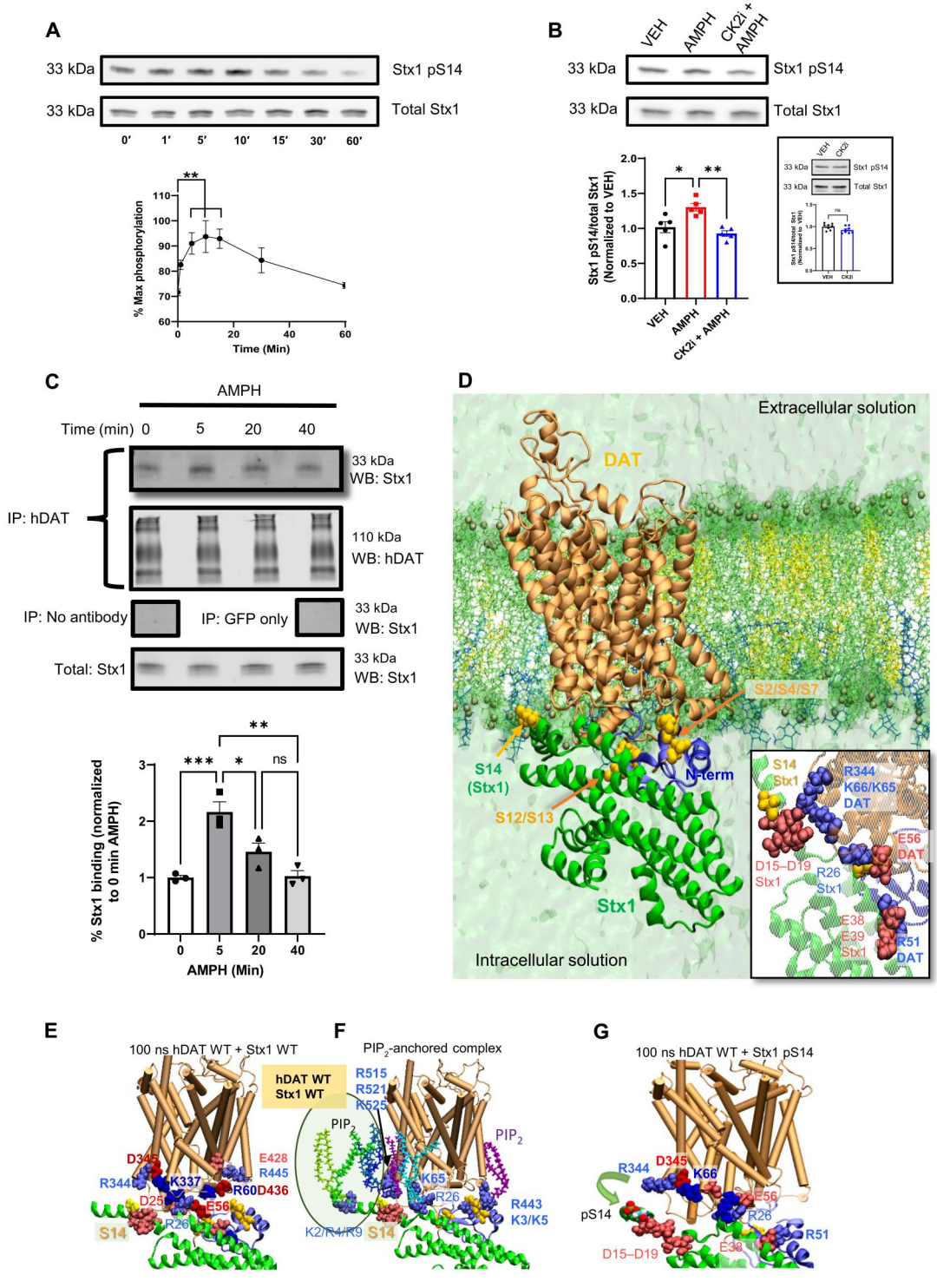

Fig. 1. AMPH promotes phosphorylation of Stx1. (**A** to **C**). Representative immunoblots (top) and quantitative analyses (bottom) of hDAT cells. (A) Ten micromolars AMPH significantly increased Stx1 phosphorylation [$F_{(6,21)}$ = 5.293, P = 0.0018, n = 4]. (B) Cells pretreated with either vehicle (VEH) or 100 nM CX-4945 (CK2i) for 6 hours and then exposed to 10 μM AMPH (or VEH) for 10 min. AMPH significantly increased Stx1 phosphorylation, and CK2i blocked this increase [$F_{(2,12)}$ = 11.06, P = 0.0019, n = 5]. Inset: CK2i (6 hours) does not affect basal Stx1 phosphorylation (t = 2.065, n = 8). (C) hDAT immunoprecipitates (IP) and western blots (WB) from cells treated with 10 μM AMPH. AMPH significantly increased hDAT-Stx1 interaction [$F_{(3,8)}$ = 17.62, n = 3, P = 0.0007]. (**D**) MD simulations of the hDAT/Stx1 complex embedded into lipids. Red and blue Van der Waals (VDW) spheres represent acidic and basic residues. Residues from DAT and Stx1 are labeled in boldface and plain face, respectively. The hDAT/Stx1 complex model predicted by ClusPro (DAT is orange with the N terminus shown in blue) was embedded into lipids (licorice) containing 1-palmitoyl-oleoyl-*sn*-glycero-3-phosphoethanolamine (POPE) and 1-palmitoyl-oleoyl-*sn*-glycero-3-phosphocholine (POPC) (green), cholesterol (CHOL) (yellow), POPS (cyan), and phosphatidylinositol 4,5-bisphosphate (PIP_2) (blue); snapshot at 10-ns equilibration. Inset: Interfacial contacts for hDAT and Stx1. (**E**) Formation of IC salt bridges R60-D436, R445-E428, and K66-D345 at 100 ns. Predicted interfacial salt bridges remained, e.g., Stx1 R26-hDAT E56 and Stx1 E38-hDAT R51. (**F**) PIP_2 coordinates some of the interaction between hDAT with Stx1. PIP_2 lipids are colored differently depending on the site of interaction (licorice format). (**G**) MD simulations at 100 ns of hDAT and Stx1 pS14. Phosphorylation of Stx1 S14 destabilized the segment pS14-D19, while the Stx1 R26-hDAT E56 salt bridge was retained. Data are means ± SEM. One-way analysis of variance (ANOVA) with Dunnett's multiple comparisons test (A) or Tukey's multiple comparisons test (B and C); Student's unpaired *t-test* (B). ns, not significant.

pS14 supports AMPH-induced DA efflux

AMPH's ability to cause DA efflux dictates its rewarding and addictive properties (*9*, *11*). Cleaving Stx1 or preventing Stx1 phosphorylation reduces AMPH-induced DA efflux, as well as AMPH-induced locomotion (*10*). Thus, it is pivotal to understand the role played by Stx1 pS14 in the reverse transport of DA. We manipulated Stx1 phosphorylation, both genetically and pharmacologically, and measured DA efflux by amperometry in hDAT cells. AMPH-induced DA efflux (represented as an upward deflection of the amperometric trace) was significantly reduced by inhibiting Stx1 phosphorylation with CK2i (Fig. 2A). Furthermore, hDAT cells expressing Stx1 S14A (prevents pS14) exhibited significantly reduced efflux compared to hDAT cells expressing Stx1 (Fig. 2B). In contrast to cells expressing Stx1, CK2 inhibition failed to reduce DA efflux in cells expressing Stx1 S14D (Asp behaves as a phosphomimetic) (Fig. 2C). These data, combined with the data in Fig. 1B, demonstrate that AMPH-induced CK2-mediated Stx1 pS14 is critical for AMPH-induced DA efflux.

Phosphorylation of hDAT N terminus and Stx1 S14 promotes constitutive DA efflux and the formation of a DAT aqueous pore in an interdependent fashion

AMPH causes Stx1 pS14 (Fig. 1A), an event required for proper DA efflux (Fig. 2) (*10*, *30*). AMPH also promotes DAT phosphorylation at the most distal N-terminal Ser (*19*–*23*). Phosphorylation of these Ser residues is required for AMPH to stimulate a robust DA efflux and associated behaviors (*18*, *21*, *22*). However, it is unclear whether these phosphorylation events regulate each other and coordinate DA efflux in an interdependent fashion by regulating the structural/functional conformations of the hDAT/Stx1 complex. To address this, we first used a combination of hDAT WT, a phosphodeficient N-terminal mutant (hDAT SA; S2A, S4A, S7A, S12A, and S13A) as well as a phosphomimetic N-terminal mutant of hDAT (hDAT SD; S2D, S4D, S7D, S12D, and S13D). First, we determined whether the phosphorylation status of the hDAT N terminus dictates the ability of AMPH to cause Stx1 pS14. In cells transfected with hDAT WT and Stx1, phosphorylation of Stx1 S14 is elevated upon AMPH exposure (Figs. 3A and 1A). However, in hDAT SA cells, AMPH fails to increase Stx1 phosphorylation (Fig. 3A). Quantitation of immunoblots is shown in Fig. 3A (bottom). These data indicate that phosphorylation of the hDAT N terminus is required for AMPH-induced Stx1 phosphorylation. Consistent with this, hDAT SD cells exhibit increased levels of Stx1 pS14 under basal conditions (fig. S2A, top). This increased Stx1 phosphorylation is not augmented by AMPH exposure (fig. S2A, top). Quantitation of the immunoblots demonstrates a significant difference in Stx1 pS14 levels between cells expressing either hDAT WT or hDAT SD (fig. S2A, bottom). We attribute this hDAT SD–mediated increase in Stx1 pS14 levels to its ability to cause cell membrane depolarization (fig. S2B). There is evidence that CK2 can be activated by membrane depolarization (*46*). Furthermore, KCl-induced membrane depolarization increases Stx1 pS14 levels, an event that is inhibited by bath application of CK2i (fig. S2C).

We found that in hDAT SD cells, rather than causing DA efflux (as observed in hDAT WT cells), AMPH initiates a downward deflection of the amperometric trace (Fig. 3B, top). This downward deflection, defined as constitutive DA efflux (CDE), has been previously observed in cells expressing hDAT genetic variations associated with autism and attention-deficit/hyperactivity disorder (*47*–*49*). The amplitude of the hDAT WT peak current, as well as hDAT SD–mediated CDE (the amplitude of CDE is defined as the maximum deflection of the amperometric current with respect to baseline), is represented in Fig. 3B (bottom). The CDE nature of the hDAT SD mutant was also confirmed by its cocaine (COC)

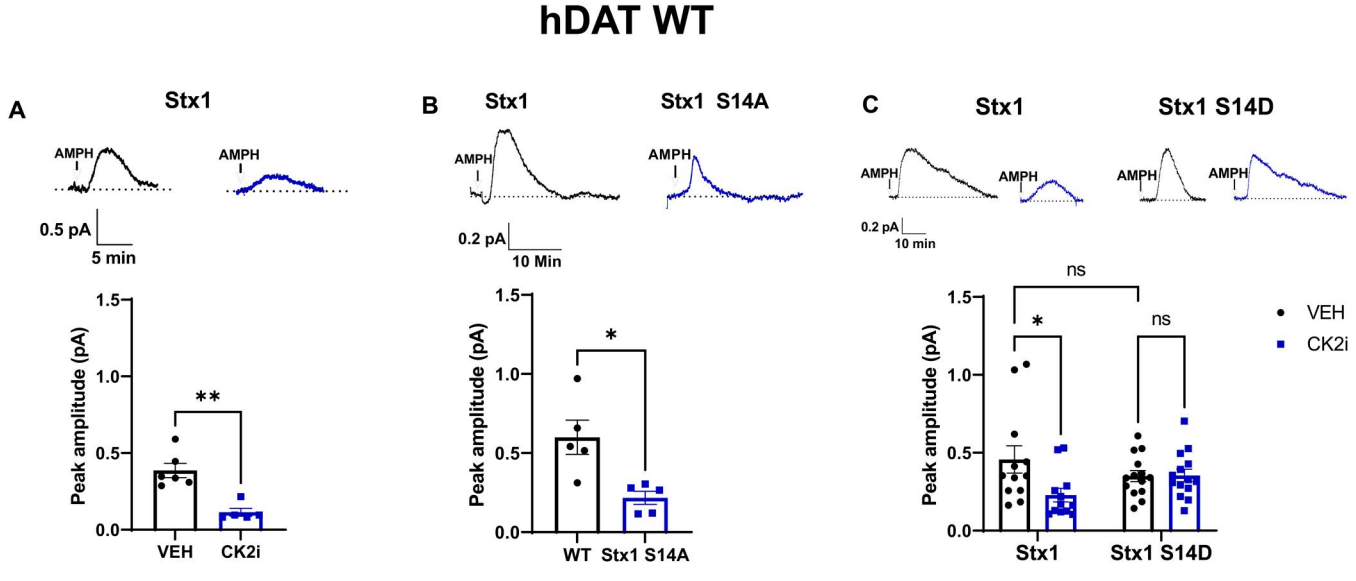

Fig. 2. Stx1 phosphorylation supports AMPH-induced DA efflux. (**A**) Top: Representative traces of AMPH-induced DA efflux in hDAT cells treated with CK2i (100 nM for 30 min) or VEH. Bottom: Quantitative analysis of peak amplitude of the amperometric currents. CK2i treatment significantly reduced DA efflux ($U = 0$, $n = 5$ to 6). (**B**) Representative traces (top) and quantitative analysis (bottom) of hDAT WT cells expressing either WT or Stx1 S14A. Stx1 S14A demonstrates a diminished ability to support DA efflux ($t = 3.307$, $n = 5$). (**C**) Representative traces (top) and quantitative analysis (bottom) of hDAT WT cells expressing either WT or Stx1 S14D. CK2i (100 nM) treatment significantly reduced DA efflux in cells expressing Stx1 but had no effect on cells expressing Stx1 S14D [$F_{(1,48)} = 4.756$ for effect of interaction, $P = 0.0341$, $n = 12$ to 14]. Data are presented as means ± SEM. Mann-Whitney test (A); Student's unpaired *t-test* (B); two-way ANOVA with Tukey's multiple comparisons test (C).

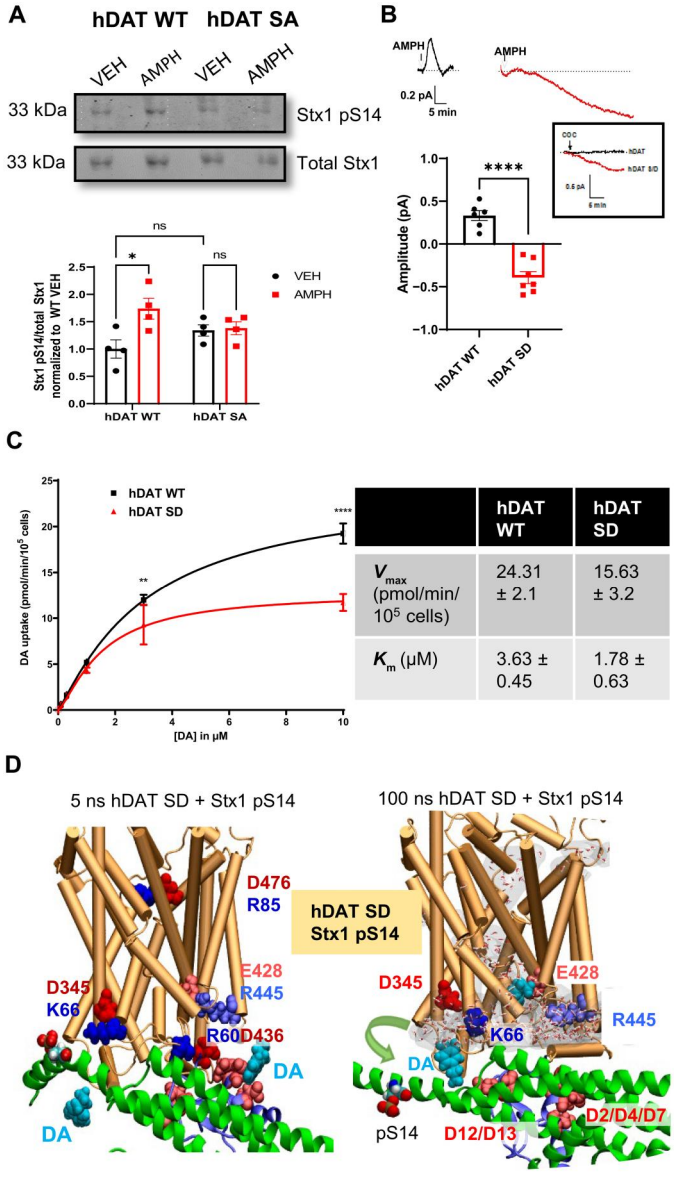

Fig. 3. hDAT N-terminus pseudophosphorylation supports CDE and the formation of an hDAT aqueous pore. (**A**) Representative immunoblot (top) and quantitative analysis (bottom) of Stx1 pS14 in hDAT WT or hDAT SA cells treated with AMPH (10 μM; 10 min). AMPH increased Stx1 pS14 only in hDAT WT. [$F_{(1,12)} = 28.04$ for effect of AMPH, $P = 0.023$; $F_{(1,12)} = 22.44$ for effect of interaction, $P = 0.038$, $n = 4$]. (**B**) Representative amperometric traces (top) and quantitative analysis (bottom) of AMPH treatment (10 μM) in hDAT WT or SD cells. AMPH causes DA efflux in hDAT WT but reveals CDE in hDAT SD cells ($t = 7.720$, $n = 6$ to 7). Inset: Representative trace of hDAT WT or hDAT SD cells treated with COC (10 μM). (**C**) ^{3}[H]DA uptake saturation curves measured from hDAT WT (black) or SD (red) cells. DA uptake for hDAT SD cells was significantly reduced compared to hDAT WT cells [$F_{(5,24)} = 7.56$, $n = 4$, $P = 0.0002$]. V_{max} was significantly reduced in hDAT SD ($t = 2.458$, $n = 4$, $P < 0.05$), while K_m was not changed ($t = 1.181$, $n = 4$). (**D**) Snapshots of MD simulation of the hDAT SD and Stx1 pS14 complex at 5 and 100 ns. Red and blue VDW spheres represent acidic and basic residues. Residues from DAT and Stx1 are labeled in boldface and plain face, respectively. pS14 and pseudophosphorylation of hDAT (SD) promote the dissociation of the hDAT K66-D345 salt bridge and reconfigures hDAT into an open, inward-facing–like conformer. DA is represented as cyan VDW spheres. Hydrated regions inside the transporter are indicated in shaded gray. Water molecules are displayed in licorice format. H_2O is shown as a ball and stick model. Data are presented as means ± SEM. Two-way ANOVA with Tukey's (A) or Bonferroni's (C) multiple comparisons test; Student's unpaired *t-test* (B and C).

sensitivity (Fig. 3B, inset). COC, a known DAT antagonist, was previously shown to block CDE (*47*, *49*). These data demonstrate that in hDAT SD cells, AMPH does not promote DA efflux but rather acts as a blocker of CDE, similar to what is observed with COC.

Next, we further characterized the functional impact of the hDAT N terminus. We performed radiolabeled [H^3]DA uptake in both hDAT WT and hDAT SD cells (Fig. 3C, top). While the Michaelis constant (K_m) was not different between the two genotypes ($P > 0.05$), V_{max} was significantly reduced in hDAT SD cells ($P < 0.05$) (Fig. 3C, bottom), a phenomenon we attribute to their ability to constitutively efflux DA, which would reduce IC accumulation of DA. To further support this, we found that this decreased [H^3]DA uptake capacity is not the result of a protein trafficking phenomenon, since hDAT SD cell surface expression is comparable to that of hDAT WT (fig. S3). Moreover, among the different combinations of hDAT/Stx1 mutants tested, only hDAT SA/Stx1 S14A displays a membrane expression that is significantly different from hDAT WT/Stx1 (fig. S3).

To understand, at the molecular level, how combined phosphorylation of hDAT N terminus and Stx1 leads to CDE, we performed MD simulations of the complex formed between hDAT SD and Stx1 pS14. Figure 3D displays snapshots at 5 and 100 ns. In Fig. 1D (inset), we show that the $D_{25}RDR_{28}$ stretch of Stx1 contributes to stabilizing the association of Stx1 with hDAT through its interaction with hDAT E56. The strength of this interaction is enhanced by S12 and S13 pseudophosphorylation (S12D and S13D) at the hDAT N terminus. Furthermore, S12D and S13D promote the formation of a salt bridge with Stx1 R26 (fig. S4) and may contribute to the experimentally observed increase in the affinity of hDAT to bind to Stx1 when exposed to AMPH (Fig. 1C). In all hDAT/Stx1 complexes tested, Stx1 D25, R26, D27, and R28 were observed to form intermittent salt bridges with hDAT K65/K337, E56/E61, K65/K337, and E61/D68, respectively. However, pseudophosphorylation of hDAT

N terminus and its increased interaction with Stx1 R26 promote the breaking of hDAT intramolecular salt bridges K66-D345 and E428-R445 (Fig. 3D, right, and fig. S4) and lead to an inward-facing conformer. In the initial configuration, hDAT was in an occluded state, in which the EC gate pair R85-D476 and three IC gating pairs R60-D436, K66-D345, and E428-R445 (*15*, *50*) were closed (Fig. 3D, left). During the simulations with hDAT SD and Stx1 pS14, these three IC salt bridges broke intermittently, leading to the opening of IC vestibule and the influx of water molecules (Fig. 3D, right, and fig. S4, A to C). Notably, one of the two displayed DA molecules (both shown in cyan space-filling), initially 25 Å away from hDAT E428 (Fig. 3D, left), migrated from the cytoplasmic solution and bound inside the IC vestibule near hDAT E428 (Fig. 3D, right), and the second diffused to bind near the IC entrance close to K66 (Fig. 3D, right). The opening probabilities of the EC gate R85-D476 and the IC gate R60-D436 were similar in all hDAT/Stx1 complexes simulated, with some of these salt bridges coordinated by PIP_2 molecules (Fig. 1F and fig. S5). However, hDAT SD, in the presence of Stx1 pS14, decreased the probability of formation of the hDAT K66-D345 salt bridge from 54 ± 20% to 17 ± 15%, promoting the opening of the hDAT IC gate. Thus, it is possible that the opening of the IC gate and the subsequent binding of DA from the cytosol near E428 and K66 is key for hDAT to transition from an uptake ready to an efflux-ready conformation and the expression of CDE. This channel-like state of the hDAT seems to be required for CDE and is dictated by the coordinated phosphorylation of both hDAT and Stx1.

In addition to structural rearrangements, phosphorylation of both hDAT and Stx1 regulates the formation of hDAT/Stx1 complex. In hDAT SD cells transfected with either Stx1, Stx1 S14A, or Stx1 S14D, we immunoprecipitated hDAT and then immunoblotted for Stx1 (fig. S6, top). The interaction between hDAT SD and Stx1 was increased by preventing (Stx1 S14A) Ser^{14} phosphorylation (fig. S6, bottom). These data support the notion that the phosphorylation status of the hDAT/Stx1 complex, in addition to causing structural rearrangements, also regulates the strength of the association between hDAT and Stx1.

Stx1 phosphorylation is required for CDE

To further understand the role of Stx1 phosphorylation in CDE, we recorded AMPH-induced DA efflux in hDAT SD cells exposed to either vehicle (VEH) or CK2i (Fig. 4A). Since hDAT SD promotes Stx1 phosphorylation (fig. S2A), it affords the opportunity to determine the role played by Stx1 pS14 in AMPH-induced DA efflux once hDAT N terminus is phosphorylated. As already described in Fig. 3B, we found that in the presence of VEH, AMPH inhibits CDE. However, in the presence of CK2i, AMPH causes a DA efflux that is comparable to what is observed in hDAT WT cells in the presence of CK2i (compare Fig. 4A to Fig. 2A). Thus, these diverse outcomes might be attributable to the different hDAT-Stx1 interactions that depend on the Stx1 phosphorylation status. Consistent with this notion, expression of Stx1 S14A in hDAT SD cells also restored the ability of AMPH to cause DA efflux (Fig. 4B). As expected, in hDAT SD cells, expression of Stx1 S14D promotes CDE, as revealed by AMPH blockade of the amperometric signal (Fig. 4B). These data indicate that upon phosphorylation of the hDAT N terminus, phosphorylation of Stx1 is necessary for the expression of CDE, a phenomenon possibly supported by the formation of an hDAT channel–like state (Fig. 3D).

We hypothesized that the reduced DA uptake observed in hDAT SD cells (Fig. 3C) was the result of CDE. Thus, inhibition of Stx1 phosphorylation, which prevents CDE, should restore normal DA uptake in hDAT SD cells. Expression of Stx1 S14A rescues the impaired [H^3]DA uptake observed in hDAT SD cells (Fig. 4C, blue line) to that of hDAT WT cells (Fig. 4C, black dotted line; these cells express Stx1). Consistent with our hypothesis, expression of Stx1 S14D impaired DA uptake in hDAT SD cells (Fig. 4C, red line). These data demonstrate that Stx1 Ser^{14} phosphorylation plays a key regulatory role in determining the functional modalities of the phosphorylated hDAT conformer (uptake versus efflux).

It is important to note that in cells expressing the phosphodeficient hDAT mutant, hDAT SA, the presence of Stx1 S14D does not promote CDE (fig. S7). These data demonstrate that phosphorylation of neither hDAT nor Stx1 alone is sufficient for the expression of CDE, but, rather, combined phosphorylation of these proteins is required for CDE to occur. Considering the results of Fig. 2 and fig. S2, they also suggest that while hDAT SD can promote Stx1 phosphorylation and CDE, Stx1 S14D is not capable of reciprocally promoting hDAT phosphorylation.

To further understand how Stx1 phosphorylation determines the different abilities of hDAT SD to respond to AMPH, we performed 100-ns MD simulations of the complex formed between hDAT SD and Stx1 S14A mutant (Fig. 4D, shown are three snapshots) and compared them to those performed for hDAT SD complexed with Stx1 pS14. Stx1 S14A substitution maintained the electrostatic interaction between hDAT SD R344 and the acidic cluster of Stx1 D15-D19 (Fig. 4D). The probability of the formation of a salt bridge between R344 and the Stx1 acidic cluster was 55 ± 25% for the complex with Stx1 S14A, compared to 15 ± 10% with Stx1 pS14. Notably, the IC gate K66-D345 salt bridge has a higher probability of forming in the complex of hDAT SD with Stx1 S14A (60 ± 25%) (Fig. 4D), compared to hDAT SD with Stx1 pS14 (17 ± 15%) (Fig. 3D). Thus, the opening of the IC gate and the formation of a translocation pathway filled with water molecules (Fig. 3D) is a process that requires both Stx1 and hDAT N terminus phosphorylation, a mechanism we believe supports the expression of CDE.

CDE occurs in *Drosophila* brain

Drosophila is a powerful model system to determine in vivo processes underlying altered DA function due to its conserved mechanisms of DA neurotransmission (*51*, *52*) and its genetic tractability. We used the *fmn Drosophila* (DAT^{fmn}) background, which lacks expression of full-length *Drosophila* DAT (dDAT) and serves as a functional knockout (*53*), in combination with phiC31-based integration, to insert an upstream activation sequence (UAS)-driven hDAT WT or hDAT SD to express these hDAT constructs specifically in DA neurons, as previously shown (*8*, *9*, *54*). We used this model system to define the role played by hDAT N terminus and Stx1 phosphorylation in AMPH-induced DA efflux ex vivo and AMPH-associated behaviors (*9*).

Using isolated fly brains expressing either hDAT WT or hDAT SD, we measured AMPH-induced DA efflux by amperometry. We excised fly brains to maintain intact DA circuitries and record DA efflux from the posterior protocerebral lateral 1 (PPL1) region, a dense cluster of DA neurons that modulate learning (Fig. 5A) (*55*, *56*). As observed in vitro (Fig. 2A), AMPH causes DA efflux in brains isolated from hDAT WT flies (Fig. 5B). Inhibition of Stx1 phosphorylation by orally administering CK2i significantly

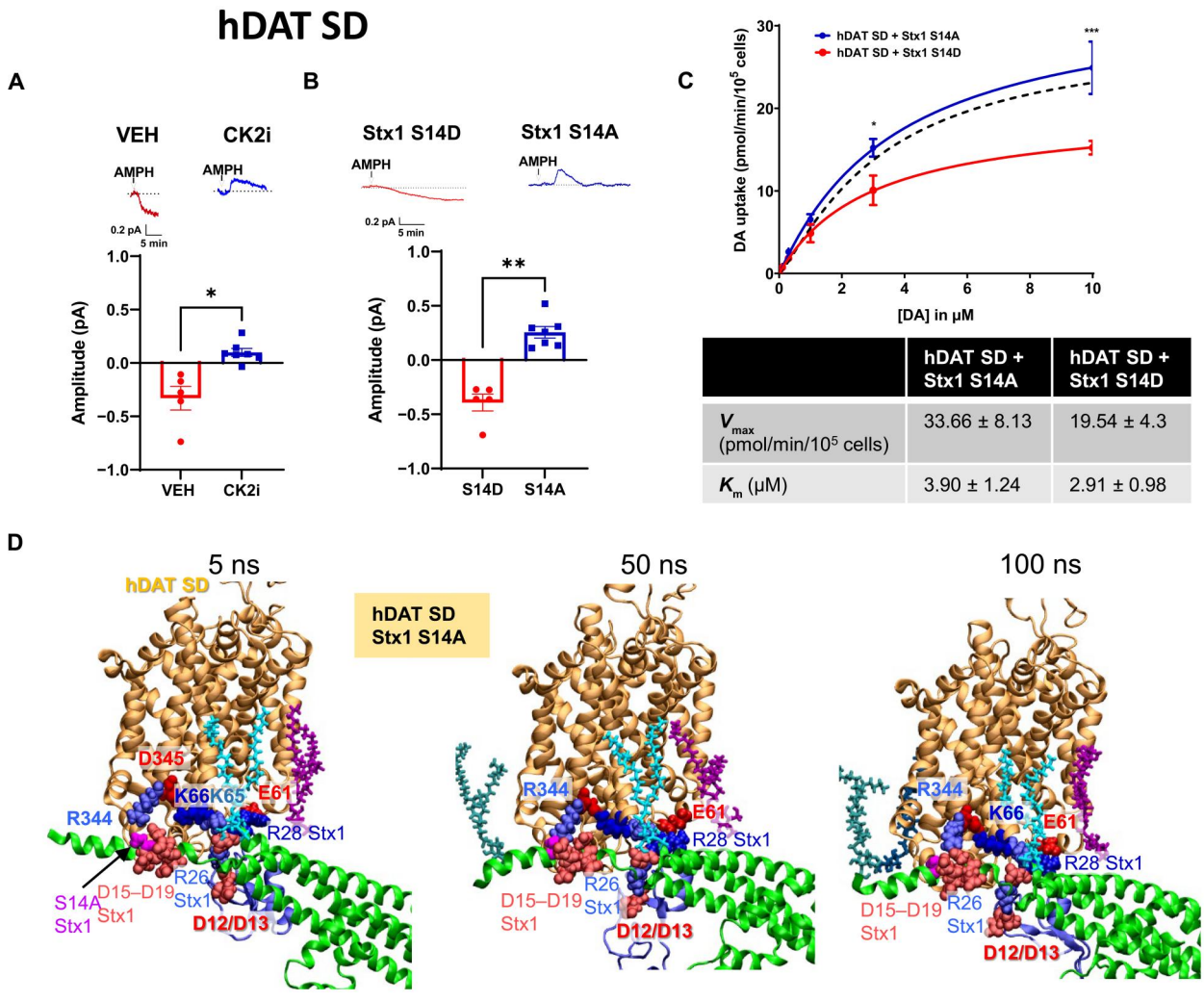

	hDAT SD + Stx1 S14A	hDAT SD + Stx1 S14D
V_{max} (pmol/min/10^5 cells)	33.66 ± 8.13	19.54 ± 4.3
K_m (µM)	3.90 ± 1.24	2.91 ± 0.98

Fig. 4. pS14 is critical for CDE. (**A**) Representative traces (top) and quantitative analysis (bottom) of the amplitude of the peak current and CDE (CDE amplitude is defined as the maximum deflection of the current from baseline) of hDAT SD cells treated with CK2i (100 nM) or VEH. CK2i treatment prevented CDE (t = 3.678, n = 5 to 7). (**B**) Representative traces (top) and quantitative analysis (bottom) of hDAT SD cells expressing either Stx1 S14D or S14A. Stx1 S14A prevented CDE (U = 0, n = 5 to 7). (**C**) Saturation curves of ^{3}[H]DA uptake measured in hDAT SD cells expressing either Stx1 S14D (red) or S14A (blue). Curves were fit to Michaelis-Menten kinetics to derive K_m and V_{max}. DA uptake for hDAT SD cells expressing Stx1 S14A was increased compared to hDAT SD cells expressing Stx1 S14D at the two highest DA concentrations used [$F_{(5,22)}$ = 4.197, n = 3 in triplicate, P = 0.0079]. The black dotted line represents hDAT WT cell uptake. (**D**) Snapshots of MD simulations of the hDAT SD/Stx1 S14A complex at 20, 50, and 100 ns. Red and blue VDW spheres represent acidic and basic residues. Residues from DAT and Stx1 are labeled in boldface and plain face, respectively. Stx1 D25, R26, D27, and R28 were observed to form intermittent salt bridges with hDAT K65/K337, D12/D13, K65/K337, and E61/D68, respectively. For clarification, some residues, e.g., Stx1 D25, hDAT D68, and K337, are not displayed. We observed this in one independent run. In each figure, the binding PIP_2 lipids are colored in licorice format. The absence of bound PIP_2 near R344 and K66 holds the association of D15 to D19 Stx1 acidic cluster with the basic cluster near hDAT R344/K66. Data are presented as means ± SEM. Student's unpaired *t-test* with Welch's correction (A); Mann-Whitney test (B); two-way ANOVA with Bonferroni's multiple comparisons test (C).

reduced the ability of AMPH to cause DA efflux (Fig. 5B). Notably, in brains isolated from hDAT SD flies, AMPH reveals a CDE (Fig. 5C), as we observed in hDAT SD cells (Fig. 3B). Furthermore, in brains of hDAT SD flies, oral treatment with CK2i restores the ability of AMPH to cause DA efflux (Fig. 5C). These data support the notion that CDE requires both Stx1 and hDAT phosphorylation. To further demonstrate that AMPH unmasks CDE by acting as an hDAT "blocker" in an ex vivo preparation, we performed parallel experiments with COC. We applied 1 µM COC to brains of both hDAT WT and hDAT SD flies. COC promoted a downward deflection of the amperometric trace exclusively in hDAT SD brains, confirming the expression of CDE in hDAT SD but not hDAT WT flies (Fig. 5D). These results demonstrate that CDE is not an in vitro epiphenomenon since it occurs in intact brain preparations.

CDE and CK2 function promote the expression of fly behaviors associated with AMPH exposure

To investigate whether CDE and CK2 activity, which induces phosphorylation of Stx1, translate to specific behaviors, we first

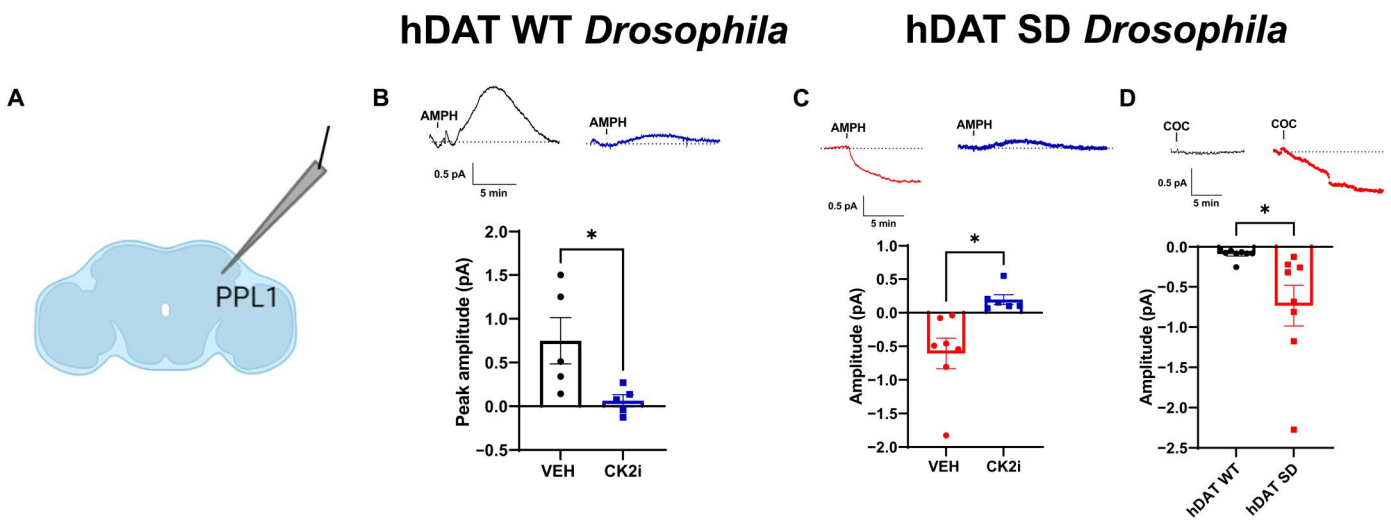

Fig. 5. Stx1 and hDAT phosphorylation status regulate DA efflux in *Drosophila* brains. (**A**) Schematic of the amperometric recordings. The amperometric electrode was positioned in the PPL1 region that is enriched in DA neurons. (**B**) Representative AMPH-induced amperometric traces (top) recorded from the PPL1 region of hDAT WT–expressing *Drosophila* brains from flies that received oral administration of VEH or CK2i (100 nM) for 24 hours and quantitative analysis of the peak currents (bottom). CK2i significantly reduced DA efflux in hDAT WT brains ($t = 2.505$, $n = 5$). (**C**) Representative AMPH-induced amperometric traces (top) recorded from hDAT SD–expressing *Drosophila* brains from flies that received oral administration of VEH or CK2i (100 nM) for 24 hours and quantitative analysis of the peak currents (bottom). CK2i significantly reduced CDE in hDAT SD brains ($t = 3.359$, $n = 6$ to 7). (**D**) Representative amperometric traces (top) recorded from the PPL1 region of hDAT WT or hDAT SD *Drosophila* brains and quantitative analysis of the peak currents (bottom). Brains were exposed acutely to COC (1 μM). COC reveals a CDE in hDAT SD that is not present in hDAT WT brains ($t = 2.528$, $n = 8$). Data are presented as means ± SEM. Student's unpaired *t-test* (B); Student's unpaired *t-test* with Welch's correction (C and D).

determined their involvement in locomotion, a basic behavior that is regulated by DA across phyla (*8*, *57*, *58*). We and others have shown that increases in EC DA levels, as a result of DA efflux, promote hyperlocomotion (*4*, *9*, *10*). Thus, we determined whether the CDE observed in hDAT SD brains translates to increased locomotion by comparing the basal locomotion of hDAT WT and hDAT SD flies. Circadian locomotor rhythmicity over 36 hours was maintained in hDAT SD flies as compared to hDAT WT flies (Fig. 6A, left). However, locomotor activity, as measured by beam crosses over a 24-hour period, was significantly increased in hDAT SD flies (Fig. 6A, right). These results are consistent with the presence of CDE in hDAT SD brains (Fig. 5C), further supporting the ability of DA efflux to regulate specific behaviors. Considering that AMPH inhibits CDE, we next measured locomotion in response to AMPH treatment in hDAT WT and hDAT SD flies (Fig. 6B). While hDAT WT flies exposed to AMPH became hyperlocomotive (Fig. 6B, left), hDAT SD flies exhibited significantly reduced locomotion in response to AMPH (Fig. 6B, right). Thus, inhibition of CDE by AMPH in hDAT SD brains (Fig. 5C) is associated with reduced hyper locomotion. Next, we determined the role played by CK2 activity in AMPH-induced locomotion in hDAT WT and hDAT SD flies. Oral administration of CK2i to hDAT WT flies inhibited the ability of AMPH to cause hyperlocomotion (Fig. 6B, left). No differences were observed between VEH and CK2i-treated flies under basal conditions (Fig. 6B, left). In contrast, in hDAT SD flies, CK2i significantly reduced basal hyperlocomotion with respect to VEH treatment, supporting the notion that CDE-induced behaviors require CK2 function (Fig. 6B, right). Moreover, CK2i exposure did not further decrease locomotion in AMPH-treated hDAT SD flies (Fig. 6B, right). Notably, treatment with CK2i did not alter COC (5 mM)–induced hyperlocomotion in flies recorded over 1 hour. Flies were treated as described in Fig. 6B, except that instead of AMPH, they received COC [VEH/VEH = 55.26 ± 6.60 beam crosses; VEH/COC = 68.02 ± 7.44 beam crosses; CK2i/VEH = 56.43 ± 7.17 beam crosses; CK2i/COC = 73.20 ± 7.97 beam crosses; $F_{(1,150)} = 3.922$, $P = 0.049$ for effect of COC; $F_{(1,150)} = 0.1810$, $P = 0.6711$ for effect of CK2i, $n = 30$ to 42], demonstrating that CK2i reduces the psychostimulant properties of AMPH but not COC.

In *Drosophila*, courting behavior is regulated by DA neurotransmission (*59*–*62*). Therefore, a drug that increases DA signaling, such as AMPH, or a process that increases EC DA levels (e.g., CDE) should alter courtship in flies. In these assays, unmated adult male flies harboring hDAT were exposed to VEH or drug and placed in a three-dimensional (3D)–printed chamber. After 10 min of acclimation, an adult unmated female fly was introduced, and behavior was video-recorded for 10 min and then scored for courtship behavior. Courtship index is calculated as the ratio of time spent demonstrating a courting behavior to total time in the chamber (see Materials and Methods). Treatment with AMPH significantly increased courtship in hDAT WT flies (Fig. 6C, left, and movies S1 and S2), underscoring that DA efflux promotes courtship. Consistent with the notion that DA efflux supports courtship, hDAT SD flies exposed to VEH also demonstrate increased courtship as compared to hDAT WT flies (Fig. 6C, right, and movie S3). This hDAT SD phenotype was reversed by treatment with CK2i (Fig. 6C, right, and movie S4), as observed for locomotion (Fig. 6B) and CDE (Fig. 5C). However, neither AMPH nor the hDAT SD mutant altered latency to courtship engagement (time it takes the male fly to begin courting the female fly) or the percentage of flies that achieved copulation (fig. S8). These data further demonstrate that CDE enhances specific fly behaviors associated

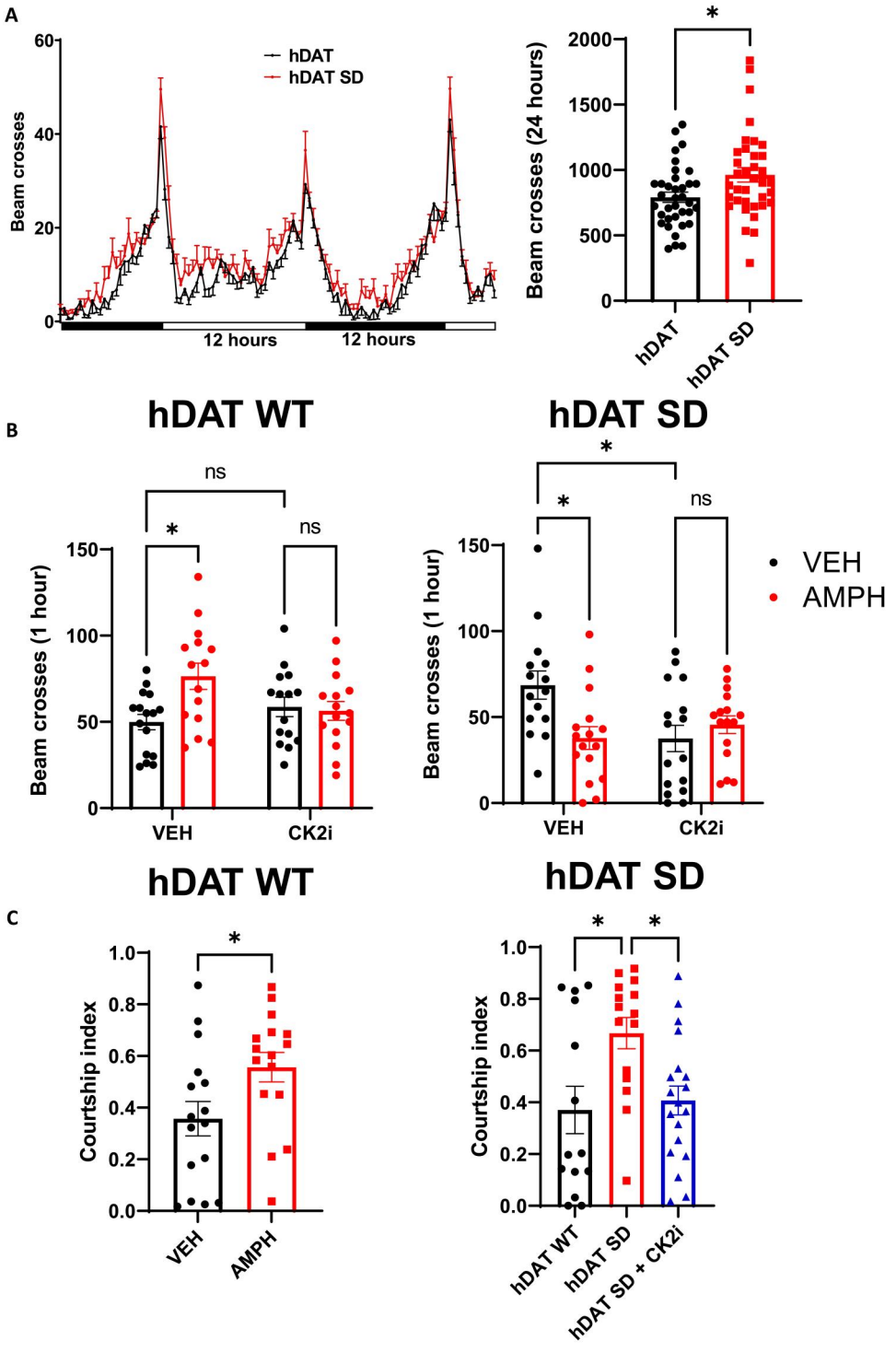

Fig. 6. CK2 activity and CDE regulate AMPH-associated behaviors in *Drosophila*. (**A**) Left: Locomotor activity was measured by beam crosses over a 36-hour period with a 12:12 light (horizontal white bar)/dark (horizontal black bar) cycle. Right: Cumulative beam crosses over 24 hours were significantly higher in the hDAT SD compared to the hDAT WT flies ($t = 2.556$, $n = 36$). (**B**) Left: hDAT WT or (right) hDAT SD *Drosophila* were orally administered VEH or CK2i (100 nM) for 24 hours. Flies were then fed either VEH (black bars) or AMPH (10 mM, red bars), and beam crosses were measured over 1 hour. AMPH significantly increased locomotion in hDAT WT flies. This increase was prevented by CK2i treatment [$F_{(1,57)} = 6.037$ for effect of interaction, $P = 0.0157$, $n = 15$ to 16]. AMPH and CK2i both significantly decreased locomotion in hDAT SD flies with respect to VEH [$F_{(1,59)} = 7.737$ for effect of interaction, $P = 0.0073$, $n = 15$ to 16]. (**C**) Courtship index was measured over a 10-min period. Left: hDAT WT virgin *Drosophila* males were fed either VEH or AMPH (10 mM) for 20 min before introduction into the 3D chamber to a virgin female hDAT WT *Drosophila*. AMPH significantly increased the courtship index ($t = 2.264$, $n = 16$). Right: hDAT WT or hDAT SD virgin *Drosophila* males were orally administered either VEH (hDAT WT and SD) or CK2i (100 nM, SD only) for 24 hours and introduced to a virgin female hDAT WT *Drosophila*. hDAT SD flies had a significantly higher courtship index than both hDAT WT and hDAT SD fed CK2i [$\chi^2(3) = 8.512$, $P = 0.0142$, $n = 14$ to 19]. Data are presented as means ± SEM. Student's unpaired *t-test* (A and C); two-way ANOVA with Tukey's multiple comparisons test (B); Kruskal-Wallis test (C).

with DA neurotransmission and that CK2 function and potentially Stx1 phosphorylation are key components in this process.

CK2 function is required for the development of AMPH preference

Reward is regulated by DA across animal species, ranging from flies to humans (*63*). The reward component of natural behavior, particularly feeding, defines how salient a specific behavioral outcome is. Psychostimulants, such as AMPH, work on DA circuits designed to respond to natural rewards. In *Drosophila*, we have shown that DA efflux is required for the manifestation of AMPH preference, a behavior used to quantify the rewarding properties of a psychostimulant (*4*, *9*). Therefore, we asked whether CK2 activity and Stx1 phosphorylation are required for AMPH preference.

We adopted a two-capillary feeding assay, developed in our laboratory, for measuring AMPH preference in *Drosophila* (*9*). In this assay, adult flies are placed in vials containing two capillaries: one containing clear sucrose and one containing blue sucrose. Flies are allowed to acclimate for 24 hours (day 1), and then baseline consumption is measured as the ratio of blue food consumed/total food consumed (day 2). A ratio of 0.5 indicates no preference. hDAT WT flies were divided into two groups and treated with either VEH or CK2i for the duration of the experiment. On day 3, either AMPH or control solution was added to blue food, and consumption in both capillaries is measured for 24 hours (Fig. 7A). Flies fed VEH showed a robust AMPH preference (red line), while flies treated with CK2i demonstrated no expression of AMPH preference (blue line; Fig. 7B). Furthermore, flies that only receive the VEH or CK2i treatment, without AMPH exposure, demonstrated no preference for clear or blue food (Fig. 7C). These results support the role of CK2 activity and, possibly, Stx1 phosphorylation, in the rewarding properties of AMPH.

As previous studies have shown, AMPHs significantly increase food consumption (*64*). In our paradigm, we see an increase in total food consumption on day 3 in both the VEH and CK2i groups that were given AMPH (Fig. 7D, left). Of note is that the AMPH-induced increase in food consumption was not significantly different between VEH and the CK2i groups. The groups that did not receive AMPH on day 3 demonstrate no increase in food consumption (Fig. 7D, right).

In Figs. 5C and 6B, we show that in hDAT SD flies, AMPH decreases locomotion and blocks CDE. Thus, we next explore whether hDAT SD flies demonstrate avoidance for AMPH. Flies were placed in vials containing two capillaries: one containing clear sucrose and

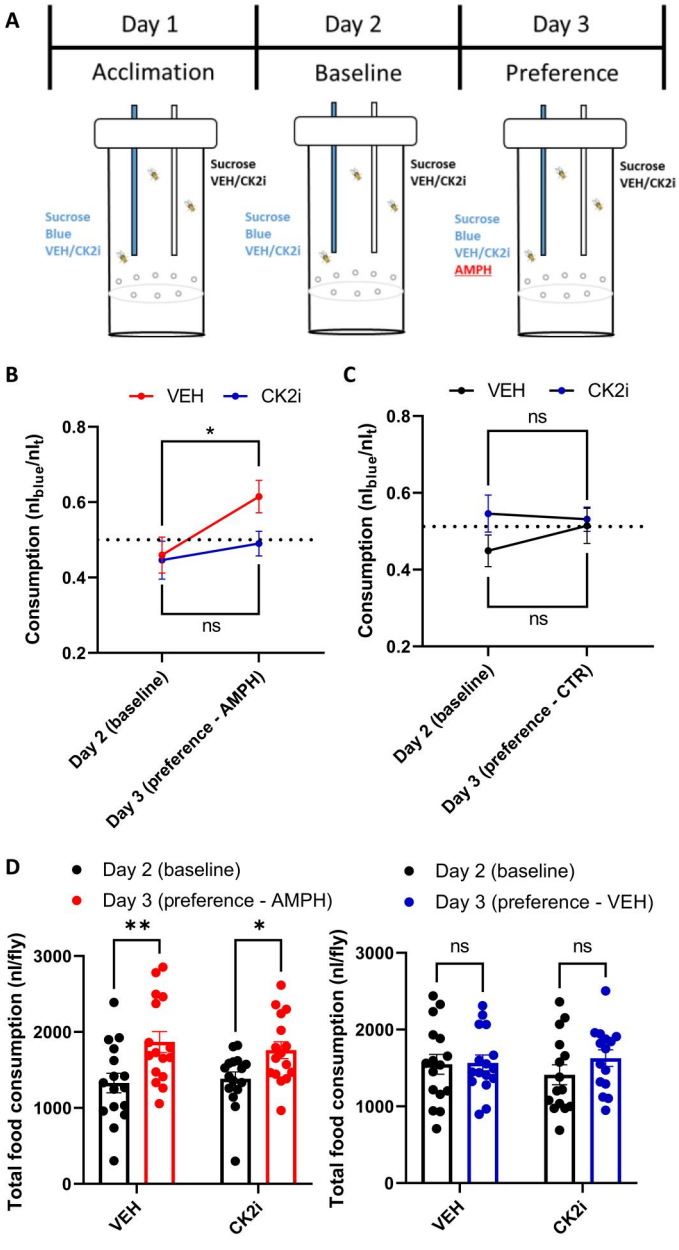

Fig. 7. CK2 activity supports AMPH preference in *Drosophila*. (**A**) Schematic of a two-choice drug consumption assay. The assay is composed of three 24-hour testing periods: acclimation, baseline, and preference. Flies were acclimated to the two-choice apparatus for 24 hours (day 1) with food (sucrose) provided in volumetric capillaries. In half of the apparatuses, the sucrose contains CK2i (100 nM), and the others have VEH. In each apparatus, one of the capillaries contains blue dye. On day 2, food consumption was recorded, and blue food consumption was normalized to the total food consumed [blue capillary/blue + transparent capillaries (nl_{blue}/nl_t)]. On day 3, AMPH (1 mM) or VEH was added to the blue capillaries. (**B**) Flies fed VEH (red line) and given the choice of AMPH consumed more from that capillary, while flies fed CK2i (100 nM, blue line) and given the choice of AMPH consumed an equal amount from both capillaries, the same as the previous day sucrose control [$F_{(1,29)} = 5.892$ for effect of day, $P = 0.0217$, $n = 15$ to 16]. (**C**) Flies were treated as above but with no AMPH. These flies demonstrated no preference for either capillary [$F_{(1,29)} = 0.4594$ for effect of day, $P = 0.5033$, $n = 15$ to 16]. (**D**) Total food consumption (clear and blue food combined) was measured. Left: Flies fed AMPH, regardless of whether they received CK2i or VEH, consumed more food on day 3 than on day 2 [$F_{(1,30)} = 17.53$, $P = 0.0002$ for effect of day; $F_{(1,30)} = 0.042$, $P = 0.8391$ for effect of drug, $n = 15$ to 16]. Right: Flies that never received AMPH show no difference in total food consumption [$F_{(1,29)} = 1.100$ for effect of day, $P = 0.3030$]. Data are presented as means ± SEM. Two-way repeated measures ANOVA with Sidak's multiple comparisons test (B to D).

one containing blue sucrose. Flies were allowed to acclimate for 24 hours (day 1), and then baseline food consumption was measured (day 2) (fig. S9A). On day 3, either AMPH or a VEH control solution was added to blue food, and food consumption in both capillaries was measured for 24 hours (fig. S9A). While hDAT SD flies treated with VEH demonstrated no preference, AMPH caused an avoidance for the blue food (fig. S9B). Of note is that AMPH did not significantly increase food consumption in hDAT SD flies, and food consumption was not significantly different between VEH and the AMPH groups (fig. S9C), pointing to a possible role played by DA efflux in regulating the ability of AMPH to increase food intake.

DISCUSSION

Stx1 is a member of the SNARE superfamily that plays a critical role in neuronal exocytosis (*26*). In addition to its role in vesicular fusion, Stx1 interacts with and regulates the function of transmembrane proteins, including ion channels and transporters (*10*, *29*–*33*). Mutations and polymorphisms in the Stx1 gene have been implicated in neuropsychiatric disorders, such as autism spectrum disorder (ASD) (*10*, *65*, *66*) and schizophrenia (*67*). Furthermore, changes in posttranslational modifications of Stx1 have also been implicated in schizophrenia. A postmortem study of the prefrontal cortex of patients with schizophrenia demonstrated deficits in both CK2 levels and Stx1 pS14 (*68*), further supporting a possible role played by Stx1 and its phosphorylation in the etiology of brain disorders. In addition to ASD and schizophrenia, Stx1 expression levels, function, and phosphorylation have also been implicated in the mechanism of action of AMPH (*10*, *30*, *32*, *69*). However, whether and how Stx1 phosphorylation supports specific behaviors associated with AMPH exposure has been largely unexplored. In this study, we defined how Stx1 phosphorylation supports the ability of AMPH to cause DA dysfunction and specific behaviors.

We demonstrate that AMPH exposure increases Stx1 pS14 levels and hDAT-Stx1 interactions, with comparable temporal dynamics, suggesting that Stx1 phosphorylation plays a pivotal role in regulating the association of Stx1 with hDAT (Fig. 1). Consistent with this, our molecular modeling shows that Stx1 S14 resides in close proximity to the acidic cluster D15 to D19, forming salt bridges with hDAT basic residues R344 and K65/K66 (Fig. 1). Thus, as discussed below, its phosphorylation might cause the structural rearrangements of the Stx1 N terminus, altering the association of the hDAT with Stx1. We also show that AMPH-induced Stx1 pS14 is CK2-mediated since CK2i inhibits this phosphorylation event (Fig. 1). The small molecule CK2i blocks CK2 activity by competing for the adenosine triphosphate binding site of the kinase, thereby inhibiting phosphorylation of Stx1 at Ser14 (*40*). It is important to note that CK2i is orally bioavailable (*70*). Previous data demonstrate that CK2 inhibition and decreased Stx1 pS14 levels selectively impair the ability of AMPH to cause DA efflux and hyperlocomotion (*10*). This impairment was also associated with altered hDAT-Stx1 association (*10*). Stx1 S14A displays an increased association with hDAT SD (fig. S6), pointing to a regulatory role of Stx1 pS14 in the formation of the hDAT/Stx1 complex. The question remains whether and how Stx1 pS14 regulates DA efflux. We first demonstrated that inhibiting Stx1 pS14, either pharmacologically (CK2i) or molecularly (Ser to Ala substitution), significantly impaired DA efflux (Fig. 2). Of note is that cells expressing the pseudophosphorylated form of Stx1 (Stx1 S14D) are resistant to the inhibitory action of CK2i, in terms of DA efflux, further reinforcing the fundamental role of CK2-mediated Stx1 phosphorylation in the reverse transport of DA. Furthermore, the lack of inhibitory actions of CK2i in cell expressing Stx1 S14D supports the notion that, for DA efflux, CK2 acts on Stx1 and not the DAT. While DAT contains putative consensus phosphorylation sequences for CK2 (*71*), to our knowledge, no evidence exists currently that CK2 directly phosphorylates DAT.

Curiously, the phosphorylation status of the hDAT N terminus also regulates the levels of Stx1 pS14. Consistent with this, preventing phosphorylation of the five hDAT most distal N-terminal Ser by their substitution to Ala (hDAT SA) inhibited the ability of AMPH to increase Stx1 pS14 levels (Fig. 3). In contrast, their pseudophosphorylation (hDAT SD) increased Stx1 pS14 levels under basal conditions (i.e., in the absence of AMPH; fig. S2A). We attribute this hDAT SD–mediated increase in Stx1 pS14 levels to its ability to cause cell membrane depolarization (fig. S2B). To further support this hypothesis, AMPH, which promotes Stx1 phosphorylation, also causes cell membrane depolarization (*13*, *17*). Furthermore, KCl-induced membrane depolarization increases Stx1 pS14 levels (fig. S2C), and there is evidence that CK2 can be activated by membrane depolarization (*46*).

It is intriguing to speculate that this AMPH-induced Stx1 phosphorylation may be supported by CaMKII function. CaMKII is a kinase that is activated by AMPH, interacts with DAT C terminus, and is required for AMPH-induced DA efflux (*21*) and behaviors (*22*). Consistent with this idea, CaMKII has been shown to act as a scaffolding protein that couples CK2 to target proteins, causing their phosphorylation (*72*). Thus, it is possible that Stx1 phosphorylation and DAT/Stx1 complex formation stem, at least in part, from the ability of AMPH to cause CaMKII activation. We have previously shown that CaMKII inhibition significantly reduces AMPH-induced DAT/Stx1 association (*30*). It is important to note that AMPH, in addition to causing DA efflux, also causes DAT plasma membrane redistribution (*73*). However, this DAT trafficking phenomenon is temporally delayed with respect to when the DAT/Stx1 complex forms and DA efflux occurs (*74*, *75*). Thus, although possible, it is unlikely that DAT trafficking is affecting the interpretation of our results.

CDE is observed upon phosphorylation of Stx1 and hDAT N terminus. It is a phenomenon that has been seen in multiple disease-associated hDAT variations, such as hDAT T356M (*49*, *76*) and hDAT A559V (*47*, *48*). In the hDAT A559V, CDE is supported, at least in part, by the ability of hDAT A559V to form an aqueous pore (*47*). hDAT SD cells, in addition to presenting increased levels of Stx1 pS14, display CDE. Thus, reverse transport of DA can occur in the absence of AMPH once both Stx1 and hDAT N terminus are phosphorylated (see also below). In hDAT SD cells, CDE was uncovered by its blockade with COC (Fig. 3B). hDAT SD–mediated CDE was also blocked by AMPH, a DAT substrate (*4*). These data suggest that while hDAT SD cells are capable of DA uptake, AMPH acts like a blocker, further pointing to Stx1 phosphorylation as a regulator of DAT function and, possibly, substrate recognition.

Our MD simulations further elucidated how the phosphorylation state of the hDAT/Stx1 complex modulates their interaction and how this might contribute to the reversal of DA transport. We determined that the hDAT-Stx1 interfacial interactions involve salt bridges between Stx1 D15/D17 and hDAT R344, Stx1

R26 and hDAT E56, and Stx1 E38/E39 and hDAT R51 (Fig. 1D). Noteworthy is that disease-associated hDAT variations resulting in the disruption of these salt bridges (e.g., R26Q in Stx1 or R51W in hDAT) have been previously implicated in altering hDAT-Stx1 interactions and DA efflux (*10*). Our 100-ns MD simulation of hDAT SD complexed with Stx1 pS14 shows that pseudophosphorylation of the hDAT N terminus promotes the breaking of hDAT salt bridges K66-D345 and E428-R445 (Fig. 3D and fig. S4) and leads to an inward-facing conformer. In this simulation, there was an influx of water molecules into the vestibule, and DA molecules migrate from the cytoplasm space to the vestibule near hDAT E428 (Fig. 3D and fig. S4, A to C). Considering that hDAT channel–like activity has been shown to support reverse transport of DA (*77*) and that Stx1 regulates this DAT function (*78*), it is possible that Stx1 and hDAT N-terminal phosphorylation promote CDE by causing, at least in part, the formation of an aqueous pore in hDAT.

The channel-like state of the hDAT SD/Stx1 pS14 complex may also contribute to the paradoxical effects seen in response to AMPH (i.e., AMPH blocks CDE). hDAT SD, in the presence of Stx1 pS14, is in a conformation that permits DA to cross the plasma membrane through an aqueous pore, down to its electrochemical gradient. Thus, it is possible that the application of EC AMPH prevents CDE by binding to the hDAT vestibule and occluding the hDAT aqueous pore. The importance of Stx1 phosphorylation in CDE is underscored by the fact that preventing Stx1 phosphorylation (Stx1 S14A) in hDAT SD cells both blocked the expression of CDE and restored, to a minimal level, the ability of AMPH to cause DA efflux (Fig. 4). Thus, Stx1 phosphorylation is essential for the expression of CDE, a functional state of hDAT characterized by reverse transport of DA, which is possibly mediated by the formation of an aqueous pore.

The role played by Stx1 phosphorylation in DA efflux in cells was also observed in isolated brains of *Drosophila*. In hDAT WT fly brains, we demonstrated that CK2 inhibition significantly inhibited DA efflux in response to AMPH (Fig. 5). Notably, as we observed in hDAT SD cells, brains of hDAT SD flies displayed an AMPH-sensitive CDE. Furthermore, in hDAT SD brains, the ability of AMPH to cause reverse transport of DA was partially restored by pharmacological inhibition of Stx1 phosphorylation (Fig. 5). These data point to the fundamental role played by Stx1 pS14 in CDE and in the ability of AMPH to cause DA efflux, not only in a heterologous expression system but also in *Drosophila* brains.

To determine the behavioral significance of both CDE and Stx1 phosphorylation, we first determined how hDAT N terminus and Stx1 phosphorylation alter locomotion in flies. Locomotion is a behavior regulated by EC DA (*57*, *58*). AMPH, by increasing EC DA, causes enhanced locomotion in both *Drosophila* and mammals (*8*, *9*, *22*, *25*, *58*). Consistent with the idea that CDE increases EC DA levels, hDAT SD flies are hyperlocomotive with respect to hDAT WT flies (Fig. 6). Furthermore, CK2 inhibition by CK2i significantly decreased the hyperlocomotion observed in hDAT SD flies to the level observed in hDAT WT flies. In hDAT SD flies, AMPH also decreases hyperlocomotion, further pointing to CDE as an hDAT function that regulates fly behaviors (Fig. 6). However, in hDAT WT flies, CK2 inhibition significantly decreased the ability of AMPH to cause hyper locomotion. Of note is that CK2i does not affect the locomotor properties of COC, further demonstrating the specificity of CK2 activity in AMPH action and ruling out a general effect on psychostimulants. These data are consistent with the ability of CK2i to significantly decrease both AMPH-induced DA efflux and CDE.

Another critical DA-associated behavior in flies is courtship (*59*–*61*). DA has been shown to both set and sustain courtship (*62*). Upon encountering a potential mate, a male decides whether or not to initiate courtship. Then, at any succeeding moment until copulation, he must decide whether or not to persevere in the courtship that has so far been unsuccessful. Males with high mating drive sustain courtship for minutes, whereas courtship by satiated males is frequently abandoned (*60*). The male′s motivation to court hinges on dopaminergic activity (*62*). Consistent with this, AMPH, by virtue of increasing EC DA levels, stimulated courtship in hDAT WT flies (Fig. 6). It is important to note that, in flies, an increase in central DA levels can reverse sexual satiety (*60*). In line with this observation, hDAT SD flies court significantly more compared to their WT counterparts (Fig. 6). This increase in sexual motivation is supported by Stx1 phosphorylation and CDE, as the significantly enhanced courtship observed by the hDAT SD flies was reduced by CK2i treatment (Fig. 6). These data are notable as AMPHs are commonly used to increase sex motivation in humans (*79*) and further demonstrates that the enhanced DA signaling promoted by Stx1 phosphorylation and the hDAT SD mutations has behavioral outcomes. While hDAT WT flies, treated with AMPH, and hDAT SD flies showed significantly increased courtship behaviors, these flies failed to have an increase in successful copulation attempts as compared to their respective controls (fig. S8). Since only the male flies in this assay were treated with the drug or harbored the hDAT pseudophosphorylation, and there were no changes in successful copulation, we surmise that the receptivity of the female flies to the male′s attempted courtship remained the same, regardless of the male′s behaviors. Since DA contributes to courtship memory (*59*), it should also be considered that hDAT SD flies and flies treated with AMPH might have altered learning in response to denial from a female.

Preference for positive reinforcers is a behavior regulated by DA in animals ranging from humans to flies (*63*). Our laboratory has recently developed a two-choice capillary assay for measuring drug preference in *Drosophila* (*9*). Using this system, we addressed the preference for AMPH in hDAT WT flies and examined how inhibiting CK2 affects AMPH preference. We demonstrated that hDAT WT flies have a robust preference for AMPH, and if the flies are treated with CK2i, this preference is significantly reduced (Fig. 7). There is a well-established link between DA release and DAT availability in reward responses in humans (*80*). Considering that CK2i inhibits the ability of AMPH to cause DA efflux (Fig. 5), these data further support a role of DA efflux in AMPH-associated behaviors and of CK2 in the expression of drug preference. AMPH treatment also significantly increased the total food consumed (food containing VEH plus food containing AMPH), regardless of VEH or CK2i treatments (Fig. 7). Even with the increased food consumption seen in the group that received AMPH, the group that received CK2i still demonstrated no preference for the drug, indicating that this increased total consumption does not play a role in the preference. Drug reinforcement measures the saliency of a specific drug exposure and is essential for the transition from drug consumption to addiction and dependence (*81*). In light of the fact that CX-4945 is showing significant promise for cancer treatment (*82*), it might also, by targeting Stx1, provide an additional therapeutic

opportunity by means of ultimately mitigating the development of AMPH use disorders.

Once DAT and Stx1 are phosphorylated, the DAT expresses channel-like activity and CDE that we associate with hyper locomotion. Both CDE and hyperlocomotion are significantly decreased by AMPH, pointing to a novel pharmacological and behavioral feature of AMPH. To further probe whether the ability of AMPH to inhibit CDE regulates more complex behaviors, we determined that AMPH in hDAT SD flies does not promote preference (fig. S9B). Instead, it causes avoidance, further demonstrating the behavioral relevance of nonvesicular DA release.

There is a clear interplay between the phosphorylation status of both hDAT and Stx1 and how this status contributes to both AMPH-induced efflux and CDE. Table S1 illustrates all the different hDAT and Stx1 phosphorylation status combinations and their experimental or predicted outcomes in terms of DA efflux. Together, these data elucidate mechanistically how Stx1 phosphorylation supports AMPH-induced DA efflux, CDE, and the role played by CK2 in AMPH-associated behaviors, including sexual motivation and drug preference.

MATERIALS AND METHODS

DNA constructs

The pEGFP vector (ClonTech, Mountain View, CA) harboring synhDAT, synhDAT SD (hDAT with Ser2, 4, 7, 12, and 13 all mutated to Asp), and synhDAT SA (hDAT with Ser2, 4, 7, 12, and 13 all mutated to Ala) coding sequences and the pcDNA3.1 vector containing Stx1, Stx1 S14A, or Stx1 S14D sequences were generated, as previously described (*10*).

Cell culture

Human embryonic kidney–293T cells were maintained in a 5% CO_2 incubator at 37°C in Dulbecco's modified Eagle's medium (DMEM) supplemented with 10% fetal bovine serum, 1 mM L-glutamine, penicillin (100 U/ml), and streptomycin (100 μg/ml). hDAT and Stx1 constructs were transiently cotransfected into these cells (hDAT cells) using Fugene-6 (Roche Molecular Biochemicals) per the manufacturer's protocol. Biochemical and electrophysiological assays were conducted 48 to 72 hours after transfection.

[^{3}H]DA uptake assays

Cells were plated on poly-D-lysine–coated 24-well plates, transiently transfected at 24 hours after plating, and then grown to ~90% confluence. *Drosophila* brains were dissected in ice-cold Schneider's *Drosophila* medium (Gibco, Waltham, MA) containing 5% bovine serum albumin (BSA) with surgical forceps. On the day of the experiment, cells or brains were washed once with 37°C KRH buffer containing 10 mM dextrose, 100 μM pargyline, 1 mM tropolone, and 100 μM ascorbic acid and equilibrated for 5 min at 37°C. Saturation kinetics of DA uptake (or single-point DA uptake) were determined using a mixture of [^{3}H]DA (PerkinElmer Life Sciences, Waltham, MA; 41.1 Ci/mmol specific activity) and unlabeled DA diluted to final DA concentrations of 0.01 to 10 μM. Uptake was initiated by bath addition of each DA dilution. Uptake was terminated after 10 min by washing cells twice in ice-cold KRH buffer. MicroScint scintillation fluid (PerkinElmer Life Sciences) was added to the wells, and the plates were counted in a TopCount scintillation counter (PerkinElmer Life Sciences). Nonspecific binding was determined in the presence of 10 μM COC. K_m and V_{max} values were derived by fitting Michaelis-Menten kinetics to the background-corrected uptake data using GraphPad Prism 9.1 (GraphPad Software, San Diego, CA). Values reported from transport studies are derived from three to five replicate experiments done in triplicate.

Cell amperometry and patch-clamp electrophysiology

Cells were washed three times with Lub's external [130 mM NaCl, 10 mM HEPES, 34 mM dextrose, 1.5 mM $CaCl_2$, 0.5 mM $MgSO_4$, 1.3 mM KH_2PO_4 (pH 7.35), and 300 to 310 mOsms/liter] bath solution at room temperature. The internal solution for the whole-cell recording contained 120 mM KCl, 10 mM NaCl, 0.1 mM $CaCl_2$, 2 mM $MgCl_2$, 1.1 mM EGTA, 10 mM HEPES, and 30 mM dextrose plus DA (2 mM or as specified in the text), adjusted to pH 7.35. Patch electrodes were pulled from quartz pipettes on a P-2000 puller (Sutter Instruments, Novato, CA) and filled with the internal solution. Whole-cell currents were recorded at a frequency of 10 kHz using an Axopatch 200B (Axon Instruments, Hawthorn, Australia) with a low-pass Bessel filter set at 1000 Hz.

For experiments using amperometry, a carbon fiber electrode connected to a second amplifier (Axopatch 200B) was placed at the plasma membrane of the cell and held at +600 mV for all experiments. The carbon fiber electrodes (ProCFE; fiber diameter is 5 μm) were obtained from Axon Instruments. For hDAT cell experiments, 10 μM AMPH was used to elicit DA efflux, while 10 μM COC was used to reveal CDE. Amperometric currents were recorded at a frequency of 100 Hz with a low-pass Bessel filter set at 10 Hz. Data were recorded and analyzed offline using pCLAMP9 software from Axon Instruments.

A sampling frequency of 100 Hz was used, and the amperometric currents were low-pass–filtered at 10 Hz. Data were recorded and analyzed offline using pCLAMP 9 software from Axon Instruments.

For experiments that involved treatment with CX-4945 (CK2i), cells were pretreated for 30 min with 100 nM CK2i (or VEH) in DMEM media. The cells were further exposed to 100 nM CK2i (or VEH) during the course of the experiment in Lub's external solution. For experiments using hDAT conditions that display impaired uptake (e.g., hDAT SD), the DA was patch-loaded into the cells (see above). For experiments comparing hDAT conditions with normal uptake (e.g., hDAT WT), DA (1 mM for 12 min) was bath-loaded into the cell in KRH [130 mM NaCl, 25 mM HEPES, 4.8 mM KCl, 1.2 mM KH_2PO4, 1.1 mM $MgSO_4$, 2.2 mM $CaCl_2$, and 10 mM D-glucose (pH 7.4)].

Western blotting protocol

Cells were washed three times with 4°C phosphate-buffered saline (Gibco) containing 1 mM EGTA and 1 mM EDTA and then lysed in radioimmunoprecipitation assay (RIPA) buffer [100 mM NaCl, 1.0% IGEPAL CA-630 (NP-40), 0.5% sodium deoxycholate, 0.1% SDS, 50 mM tris, and 100 μM phenylmethylsulfonyl fluoride (pH 8.0)] supplemented with a protease inhibitor cocktail at a 1:100 dilution (P8340, Sigma-Aldrich, St. Louis, MO). Lysates were passed twice through a 27.5-gauge needle and centrifuged at 15,000*g* for 30 min. Supernatants were then separated by 10% SDS–polyacrylamide gel electrophoresis (SDS-PAGE) gel, transferred to polyvinylidene difluoride (PVDF) membrane (Millipore, Bedford, Massachusetts), and immunoblotted. Blocking was done with either Intercept blocking buffer (LI-COR, Lincoln, Nebraska) or

4% milk. Primary antibodies used targeted hDAT (1:1000; MAB369 Millipore, Burlington, MA), Stx1 (1:1000; S0664 Sigma-Aldrich), pS14 Stx1 (1:1000; ab63571 Abcam, Cambridge, UK), and β-actin (1:1000; A2228, Sigma-Aldrich). Secondary antibodies were goat anti-rat horseradish peroxidase–conjugated (1:5000; Jackson ImmunoResearch, West Grove, PA), goat anti-rabbit immunoglobulin G (IgG) 680RD (1:10000; 926-68071, LI-COR), goat anti-mouse IgG 800CW (1:10000; 926-32210, LI-COR), or goat anti-rat IgG 800CW (1:10000; 926-32219, LI-COR). Band densities were quantified using ImageJ or Image Studio (LI-COR), and data from three to four separate experiments were combined.

Immunoprecipitation assays

Cells were grown and lysed in the same manner as above for Western blots, except that tris-buffered saline (TBS; pH 7.4) with 1% Triton X-100 (TBS-Triton) was used to lyse the cells. A portion of the total cell supernatant was collected to analyze for total protein. The remaining supernatant was incubated at 4°C for 1 hour with Sepharose-G beads (Thermo Fisher Scientific), previously washed with 5% BSA in TBS-Triton buffer, and preincubated overnight with 2.5 μg anti–green fluorescent protein (GFP) antibody ab290 (Abcam). For the negative control, the supernatant was incubated with BSA-blocked Sepharose-G beads alone (no antibody). As an additional control, lysate from mock-transfected cells was incubated at 4°C for 1 hour with Sepharose-G beads (Thermo Fisher Scientific), previously washed with 5% BSA in TBS-Triton buffer, and preincubated with 2.5 μg of anti-GFP antibody. Beads were spun down and washed with cold RIPA buffer, and samples were eluted first with sample buffer (1% SDS, 18% glycerol, 0.05% phenol blue, 62.5 mM tris HCl, 7 M urea, 2 M thiourea, and 0.1 M dithiothreitol) at 95°C for 5 min and then thiourea/urea mixture (7 M urea and 2 M thiourea) at 95°C for 5 min. Total lysates and eluates were analyzed by SDS-PAGE and immunoblotting (see above for antibody details). Band intensity was quantified using Image Studio (LI-COR). The association between Stx1 variants and hDAT variants was represented as the ratio of eluate/total lysate band intensity, normalized to the eluate/total lysate ratio observed in hDAT WT with VEH condition and expressed as a percentage.

Biotinylation assays

Cells were grown and lysed in the same manner as the above methods for Western blots. On the day of the assay, cells were washed three times with 4°C phosphate-buffered saline (Gibco), and then sulfosuccinimidyl-2-(biotinamido)ethyl-1,3-dithiopropionate-biotin (1.0 mg/ml; Pierce, Rockford, IL) was added to each well and allowed to incubate for 30 min at 4°C. Cells were quenched with 100 mM glycine and then solubilized in RIPA buffer (see above for details) for 30 min at 4°C. Extracts were collected from wells and centrifuged for 30 min at 15,000*g* at 4°C. The supernatant was added to immunopure immobilized streptavidin beads (Pierce). Beads were allowed to incubate for 45 min at room temperature and were extensively washed, after which Laemmli buffer with 2-mercaptoethanol was added to the spun-down beads. The eluent from the beads, as well as the biotinylated input (5 μg), was run on an SDS-PAGE gel, transferred to a PVDF membrane (Millipore), and immunoblotted (see above for antibody details). Band densities were quantified using ImageJ or Image Studio (LI-COR). Surface expression was represented as surface/total band intensity and normalized to the ratio observed in hDAT WT-Stx1 group and expressed as a percentage. Data from four separate experiments were combined.

Drosophila rearing and stocks

All *Drosophila melanogaster* lines were maintained on standard cornmeal-molasses fly food (Nutrifly) at 25°C under a 12:12-hour light-dark schedule. Fly stocks include tyrosine hydroxylase (TH)–GAL4 [Bloomington Indiana Stock Center (BI) 8848], $DAT^{MB07315}$ (BI 25547), w^{1118} (BI 6326), UAS-mCherry (Kyoto Stock Center 109594), M[vas-int.Dm]ZH-2A; (M[3xP3-RFP.attP′]ZH-22A (Bl 24481), and DAT^{fmn} (dDAT KO). *Drosophila* expressing homozygous DAT^{fmn} (dDAT KO), TH-GAL4, and UAS-mCherry were outcrossed to a control line (w^{1118}) for 5 to 10 generations. The transgenes (hDAT WT and hDAT SD) were cloned into pBID-UASC, and constructs were injected into embryos from M[vas-int.Dm]ZH-2A; (M[3xP3-RFP.attP′]ZH-22A. Flies containing transgenes were outcrossed to dDAT KO flies (in w^{1118} background) for 5 to 10 generations. Adult male flies (2 to 6 days after eclosion) containing a single copy of hDAT WT or hDAT SD in DA neurons in the DAT^{fmn} background were used for all behavior and electrophysiological experiments (adult female flies also used during the courtship assay; see below).

Drosophila brain amperometry

Drosophila brains from hDAT WT or hDAT SD flies were dissected in cold Schneider′s *Drosophila* medium (Gibco). Brains were transferred to a 35 mM Sylgard dish with 3 ml of Lub′s external solution (see above for details) and pinned to the plate using tungsten wire (California Fine Wire Company, Grover Beach, California). A carbon fiber electrode connected to an Axopatch 200B amplifier (Axon Instruments) was held at +600 mV and was placed into the TH-positive PPL1 DA neuron region, guided by mCherry fluorescence. For *Drosophila* brain amperometry experiments, 20 μM AMPH was used to elicit DA efflux, while 1 μM COC was used to reveal CDE. The electrode, equipment, and filtering parameters were the same as used in the cell experiments (see above). Data were recorded and analyzed offline using pCLAMP 9 from Axon Instruments.

Drosophila locomotion

Unmated adult male flies (2 to 3 days after eclosion) were collected, anesthetized with CO_2, and transferred to glass tubes with standard fly food. The *Trikinetics Drosophila* Activity Monitoring System (Waltham, Massachusetts) was used to measure locomotion. For circadian locomotion, after 24 hours of acclimation, locomotion was recorded for 24 hours by beam breaks. For the AMPH- or COC-induced locomotion, flies were pretreated for 24 hours with either VEH [dimethyl sulfoxide (DMSO)] or 100 nM CK2i in standard fly food. Flies were then fed standard fly food with AMPH (10 mM) or COC (5 mM) and either VEH or CK2i, and after 1 hour of acclimation, beam breaks were measured as above for a period of 1 hour.

Drosophila courtship

Drosophila courtship was measured in a custom 3D-printed chamber (33 mm by 10 mm by 10 mm).

AMPH-induced courtship

Adult male flies (2 to 6 days after eclosion) were starved for 6 hours in a vial with 1% agar. Flies were then fed standard fly food containing 10 mM AMPH (or VEH) for 20 min. Male flies were placed into the chamber for 10 min of acclimation before the introduction of an adult female fly (2 to 6 days after eclosion). Courtship was recorded for 10 min (Sony, Exmore R Optical SteadyShot).

CK2i courtship

Adult male flies were fed standard fly food containing 100 nM CK2i (or VEH) for 24 hours before courtship. Male flies were placed into the 3D-printed chamber, and the same acclimation and recording protocol as above were performed.

All courtship videos were scored blinded to the genotype and drug treatment. Video scorers manually timed and recorded the time spent displaying one of five courtship behaviors (following, wing extension, abdomen bend, tapping, and attempted copulation). The courtship index was calculated as the fraction of the amount of time the male spent courting the female over the total 10 min. Latency to court was measured as the duration of time between the introduction of the female and displaying of courtship behavior by the male. Achievement of copulation was recorded and used for analysis.

Drosophila two-choice assays

A custom two-choice apparatus was constructed to measure drug preference at the nanoliter level in *Drosophila*. Each apparatus contained two volumetric capillaries: one with clear food (100 mM sucrose) and one with blue food (100 mM sucrose, 500 μM blue dye). Half of the groups also received CK2i (100 nM) in both capillaries, while half of the groups received VEH (DMSO) in both capillaries. Food consumption was measured every 24 hours, and capillaries were refilled and replaced. Adult male flies (2 to 5 days after eclosion) were anesthetized by CO_2, transferred to the apparatus, and given 24 hours to acclimate to the liquid capillary food. The following 24 hours were used to calculate the baseline preference for clear and blue food. To determine AMPH preference, on the third day, the blue capillary was supplemented with 1 mM AMPH (see Fig. 7A). Preference was calculated as consumption of blue food over total consumption (blue food and clear food together).

Molecular modeling of Stx1 and Stx1-CK2 binary complex

Human Stx1 (Q16623) structural models (residues 1 to 260) were constructed using Robetta (*42*), based on Stx1 in a closed conformation (*83*)[Protein Data Bank (PDB): 4JEH], and the missing loop (residues 1 to 26) in Stx1 was modeled by Robetta. Using the top five Stx1 models, we performed protein-protein docking simulations for each Stx1 model against the hCK2 (V11-V328) crystal structure (PDB: 3U4U) (*84*) using ClusPro (*43*). We selected one Stx1 model for further study, in which the hCK2 catalytic residue D156 is in the proximity of Stx1 S14 [known phosphorylation site (*34*); see fig. S1A].

Modeling of hDAT-Stx1 complex structure

The full-length hDAT in an occluded conformation was taken from a previous study (*9*, *41*). We generated a series of structural models for the hDAT-Stx1 binary complex using ClusPro (*43*). We used occluded/closed states of hDAT and Stx1 as conformers. One thousand models were generated, which were grouped in 30 clusters based on their structural similarities. These were rank-ordered on the basis of cluster size (accounting for favorable entropic effects) and further sorted following three criteria specific to the hDAT-Stx1 complex in a lipid environment: (i) Stx1 should bind from the IC region (i.e., EC-bound forms were excluded); (ii) the hDAT-Stx1 complex should have proper orientation of the aromatic residues (i.e., Trp) on the EC and IC sides to enable suitable anchoring into the lipids; and (iii) residues (e.g., Stx1 R26 and hDAT R51), whose mutations have been shown to alter hDAT-Stx1 interactions in a previous study (*10*), should be involved directly or indirectly in interfacial contacts. Notably, the most energetically favorable model, predicted by ClusPro, satisfied these three criteria and, thus, was selected for further investigation using MD simulations (see Fig. 1D).

MD simulations of hDAT-Stx1 complex in the neuronal lipid environment

Three simulation systems were constructed using the CHARMM-GUI Membrane Builder module (*85*), based on the ClusPro-predicted binary complex model, and simulations of 100 ns each were conducted in triplicate for each system: (i) hDAT SD + Stx1 S14A; (ii) hDAT WT + Stx1 pS14, in which Stx1 S14 was phosphorylated; (iii) hDAT SD + Stx1 pS14, in which Stx1 S14 was phosphorylated; and (iv) hDAT WT + Stx1 WT.

For each system, the protein complex was embedded into neuronal membrane/lipids composed of 1-palmitoyl-oleoyl-*sn*-glycero-3-phosphoethanolamine (POPE) and 1-palmitoyl-oleoyl-*sn*-glycero-3-phosphocholine (POPC), cholesterol (CHOL), palmitoyl-oleoyl-phosphatidylinositol, and PIP_2 using the CHARMM-GUI Membrane Builder module (*85*). The lipid composition was adapted from a previous study (*44*) to account for the asymmetric lipid distribution of neuronal membranes: The outer lipid layer contained POPC (35%), POPE (35%), and CHOL (30%); the inner contained POPC (20%), POPE (25%), CHOL (25%), PIP_2 (15%), and POPS (15%). Fully equilibrated transferable intermolecular potential 3P waters were added to build a simulation box of 136 Å by 136 Å by 167 Å. Na^+ and Cl^- ions were added to obtain a 0.15 M NaCl neutral solution. Each simulation system contained approximately 291,000 atoms, including those of the hDAT-Stx1 complex, 570 lipid molecules, and 70,000 water molecules. A typical MD simulation setup is shown in Fig. 1D. For the system (*3*), i.e., hDAT SD + Stx1 pS14, 10 DA molecules were distributed to both EC and IC solutions. All simulations were performed using NAMD (*86*) following the previous protocol (*44*). The probability of selected interactions was assessed by counting the times of atom-atom interactions within a distance of 4 Å for the examined amino acid pair at 0.2-ns intervals during 100-ns trajectories. VMD (*87*) with in-house scripts was used for visualization and trajectory analysis.

Statistical analyses

Experiments were designed after statistical power calculations based on preliminary data using GPower 3.1. Statistical analyses were run on GraphPad Prism 9.1. Shapiro-Wilk normality tests were performed to ensure that data were normally distributed, and Bartlett's tests were performed to check for heteroscedasticity. If data failed these assumptions, the proper nonparametric tests were used. Unpaired *t-tests* were used for all comparisons between two groups, and Welch's correction was used whenever the variances significantly differed between groups. When using one-way or two-way analyses of variance (ANOVAs), Tukey's post hoc was used in

most cases. However, in the scenario where all means were being compared to a control mean, Dunnett's post hoc was used. In the case that the post hoc comparisons were only done between the different concentrations between groups, such as in the kinetic uptake experiments, Bonferonni's post hoc was used. For all repeated measures two-way ANOVAs, Sidak's multiple comparisons post hoc was used. For categorical data, the chi-square test was used. Mantel-Cox log-rank survival analysis was used for all survival plots. For all experiments, $^{*}P < 0.05$, $^{**}P < 0.01$, $^{***}P < 0.001$, and $^{****}P < 0.0001$.

Supplementary Materials

This PDF file includes:
Figs. S1 to S9
Table S1

Other Supplementary Material for this manuscript includes the following:
Movies S1 to S4
Raw Numerical Data
Raw Modeling Material

View/request a protocol for this paper from *Bio-protocol*.

REFERENCES AND NOTES

1. S. Kutcher, M. Aman, S. J. Brooks, J. Buitelaar, E. van Daalen, J. Fegert, R. L. Findling, S. Fisman, L. L. Greenhill, M. Huss, V. Kusumakar, D. Pine, E. Taylor, S. Tyano, International consensus statement on attention-deficit/hyperactivity disorder (ADHD) and disruptive behaviour disorders (DBDs): Clinical implications and treatment practice suggestions. *Eur. Neuropsychopharmacol.* **14**, 11–28 (2004).
2. D. Vearrier, M. I. Greenberg, S. N. Miller, J. T. Okaneku, D. A. Haggerty, Methamphetamine: History, pathophysiology, adverse health effects, current trends, and hazards associated with the clandestine manufacture of methamphetamine. *Dis. Mon.* **58**, 38–89 (2012).
3. T. N. A. Winkelman, L. K. Admon, L. Jennings, N. D. Shippee, C. R. Richardson, G. Bart, Evaluation of amphetamine-related hospitalizations and associated clinical outcomes and costs in the United States. *JAMA Netw. Open* **1**, e183758 (2018).
4. D. Sulzer, M. S. Sonders, N. W. Poulsen, A. Galli, Mechanisms of neurotransmitter release by amphetamines: A review. *Prog. Neurobiol.* **75**, 406–433 (2005).
5. Z. Freyberg, M. S. Sonders, J. I. Aguilar, T. Hiranita, C. S. Karam, J. Flores, A. B. Pizzo, Y. Zhang, Z. J. Farino, A. Chen, C. A. Martin, T. A. Kopajtic, H. Fei, G. Hu, Y. Y. Lin, E. V. Mosharov, B. D. McCabe, R. Freyberg, K. Wimalasena, L.-W. Hsin, D. Sames, D. E. Krantz, J. L. Katz, D. Sulzer, J. A. Javitch, Mechanisms of amphetamine action illuminated through optical monitoring of dopamine synaptic vesicles in Drosophila brain. *Nat. Commun.* **7**, 10652 (2016).
6. D. Sulzer, How addictive drugs disrupt presynaptic dopamine neurotransmission. *Neuron* **69**, 628–649 (2011).
7. M. Jaber, S. Jones, B. Giros, M. G. Caron, The dopamine transporter: A crucial component regulating dopamine transmission. *Mov. Disord.* **12**, 629–633 (1997).
8. P. J. Hamilton, A. N. Belovich, G. Khelashvili, C. Saunders, K. Erreger, J. A. Javitch, H. H. Sitte, H. Weinstein, H. J. G. Matthies, A. Galli, PIP2 regulates psychostimulant behaviors through its interaction with a membrane protein. *Nat. Chem. Biol.* **10**, 582–589 (2014).
9. A. N. Belovich, J. I. Aguilar, S. J. Mabry, M. H. Cheng, D. Zanella, P. J. Hamilton, D. J. Stanislowski, A. Shekar, J. D. Foster, I. Bahar, H. J. G. Matthies, A. Galli, A network of phosphatidylinositol (4,5)-bisphosphate (PIP_2) binding sites on the dopamine transporter regulates amphetamine behavior in *Drosophila Melanogaster*. *Mol. Psychiatry* **26**, 4417–4430 (2021).
10. E. Cartier, P. J. Hamilton, A. N. Belovich, A. Shekar, N. G. Campbell, C. Saunders, T. F. Andreassen, U. Gether, J. Veenstra-Vanderweele, J. S. Sutcliffe, P. G. Ulery-Reynolds, K. Erreger, H. J. G. Matthies, A. Galli, Rare autism-associated variants implicate syntaxin 1 (STX1 R26Q) phosphorylation and the dopamine transporter (hDAT R51W) in dopamine neurotransmission and behaviors. *EBioMedicine* **2**, 135–146 (2015).
11. A. Salahpour, A. J. Ramsey, I. O. Medvedev, B. Kile, T. D. Sotnikova, E. Holmstrand, V. Ghisi, P. J. Nicholls, L. Wong, K. Murphy, S. R. Sesack, R. M. Wightman, R. R. Gainetdinov, M. G. Caron, Increased amphetamine-induced hyperactivity and reward in mice overexpressing the dopamine transporter. *Proc. Natl. Acad. Sci. U.S.A.* **105**, 4405–4410 (2008).
12. M. S. Sonders, S. J. Zhu, N. R. Zahniser, M. P. Kavanaugh, S. G. Amara, Multiple ionic conductances of the human dopamine transporter: The actions of dopamine and psychostimulants. *J. Neurosci.* **17**, 960–974 (1997).
13. H. H. Sitte, S. Huck, H. Reither, S. Boehm, E. A. Singer, C. Pifl, Carrier-mediated release, transport rates, and charge transfer induced by amphetamine, tyramine, and dopamine in mammalian cells transfected with the human dopamine transporter. *J. Neurochem.* **71**, 1289–1297 (1998).
14. D. Joseph, S. Pidathala, A. K. Mallela, A. Penmatsa, Structure and gating dynamics of Na^+/Cl^- coupled neurotransmitter transporters. *Front. Mol. Biosci.* **6**, 80 (2019).
15. M. H. Cheng, I. Bahar, Molecular mechanism of dopamine transport by human dopamine transporter. *Structure* **23**, 2171–2181 (2015).
16. C. S. Karam, J. A. Javitch, Phosphorylation of the amino terminus of the dopamine transporter: Regulatory mechanisms and implications for amphetamine action. *Adv. Pharmacol.* **82**, 205–234 (2018).
17. H. Khoshbouei, H. Wang, J. D. Lechleiter, J. A. Javitch, A. Galli, Amphetamine-induced dopamine efflux. A voltage-sensitive and intracellular Na^+–dependent mechanism. *J. Biol. Chem.* **278**, 12070–12077 (2003).
18. H. Khoshbouei, N. Sen, B. Guptaroy, L. A. Johnson, D. Lund, M. E. Gnegy, A. Galli, J. A. Javitch, N-terminal phosphorylation of the dopamine transporter is required for amphetamine-induced efflux. *PLOS Biol.* **2**, E78 (2004).
19. J. D. Foster, B. Pananusorn, R. A. Vaughan, Dopamine transporters are phosphorylated on N-terminal serines in rat striatum. *J. Biol. Chem.* **277**, 25178–25186 (2002).
20. C. S. Karam, N. Sen, J. A. Javitch, Phospho-specific antibodies targeting the amino terminus of the human dopamine transporter. *J. Chem. Neuroanat.* **83-84**, 91–98 (2017).
21. J. U. Fog, H. Khoshbouei, M. Holy, W. A. Owens, C. B. Vaegter, N. Sen, Y. Nikandrova, E. Bowton, D. G. McMahon, R. J. Colbran, L. C. Daws, H. H. Sitte, J. A. Javitch, A. Galli, U. Gether, Calmodulin kinase II interacts with the dopamine transporter C terminus to regulate amphetamine-induced reverse transport. *Neuron* **51**, 417–429 (2006).
22. A. B. Pizzo, C. S. Karam, Y. Zhang, C. L. Ma, B. D. McCabe, J. A. Javitch, Amphetamine-induced behavior requires CaMKII-dependent dopamine transporter phosphorylation. *Mol. Psychiatry* **19**, 279–281 (2014).
23. Q. Wang, N. Bubula, J. Brown, Y. Wang, V. Kondev, P. Vezina, PKC phosphorylates residues in the N-terminal of the DA transporter to regulate amphetamine-induced DA efflux. *Neurosci. Lett.* **622**, 78–82 (2016).
24. C. Granas, J. Ferrer, C. J. Loland, J. A. Javitch, U. Gether, N-terminal truncation of the dopamine transporter abolishes phorbol ester- and substance P receptor-stimulated phosphorylation without impairing transporter internalization. *J. Biol. Chem.* **278**, 4990–5000 (2003).
25. A. B. Pizzo, C. S. Karam, Y. Zhang, H. Yano, R. J. Freyberg, D. S. Karam, Z. Freyberg, A. Yamamoto, B. D. McCabe, J. A. Javitch, The membrane raft protein Flotillin-1 is essential in dopamine neurons for amphetamine-induced behavior in *Drosophila*. *Mol. Psychiatry* **18**, 824–833 (2013).
26. M. K. Bennett, N. Calakos, R. H. Scheller, Syntaxin: A synaptic protein implicated in docking of synaptic vesicles at presynaptic active zones. *Science* **257**, 255–259 (1992).
27. I. Dulubova, S. Sugita, S. Hill, M. Hosaka, I. Fernandez, T. C. Südhof, J. Rizo, A conformational switch in syntaxin during exocytosis: Role of munc18. *EMBO J.* **18**, 4372–4382 (1999).
28. J. Pevsner, S. C. Hsu, R. H. Scheller, n-Sec1: A neural-specific syntaxin-binding protein. *Proc. Natl. Acad. Sci. U.S.A.* **91**, 1445–1449 (1994).
29. R. D. Blakely, U. Sung, SNARE-ing neurotransmitter transporters. *Nat. Neurosci.* **3**, 969–971 (2000).
30. F. Binda, C. Dipace, E. Bowton, S. D. Robertson, B. J. Lute, J. U. Fog, M. Zhang, N. Sen, R. J. Colbran, M. E. Gnegy, U. Gether, J. A. Javitch, K. Erreger, A. Galli, Syntaxin 1A interaction with the dopamine transporter promotes amphetamine-induced dopamine efflux. *Mol. Pharmacol.* **74**, 1101–1108 (2008).
31. C. Dipace, U. Sung, F. Binda, R. D. Blakely, A. Galli, Amphetamine induces a calcium/calmodulin-dependent protein kinase II-dependent reduction in norepinephrine transporter surface expression linked to changes in syntaxin 1A/transporter complexes. *Mol. Pharmacol.* **71**, 230–239 (2007).
32. A. Lanzo, A. Lanzo, B. D. Safratowich, S. R. Kudumala, I. Gallotta, G. Zampi, E. D. Schiavi, L. Carvelli, Silencing of *Syntaxin 1A* in the dopaminergic neurons decreases the activity of the dopamine transporter and prevents amphetamine-induced behaviors in *C. elegans*. *Front Physiol.* **9**, 576 (2018).
33. O. Fili, I. Michaelevski, Y. Bledi, D. Chikvashvili, D. Singer-Lahat, H. Boshwitz, M. Linial, I. Lotan, Direct interaction of a brain voltage-gated K^+ channel with syntaxin 1A: Functional impact on channel gating. *J. Neurosci.* **21**, 1964–1974 (2001).
34. T. Dubois, P. Kerai, M. Learmonth, A. Cronshaw, A. Aitken, Identification of syntaxin-1A sites of phosphorylation by casein kinase I and casein kinase II. *Eur. J. Biochem.* **269**, 909–914 (2002).

35. C. Borgo, C. D'Amore, S. Sarno, M. Salvi, M. Ruzzene, Protein kinase CK2: A potential therapeutic target for diverse human diseases. *Signal Transduct. Target. Ther.* **6**, 183 (2021).
36. K.-H. Lee, M.-Y. Kim, D.-H. Kim, Y.-S. Lee, Syntaxin 1A and receptor for activated C kinase interact with the N-terminal region of human dopamine transporter. *Neurochem. Res.* **29**, 1405–1409 (2004).
37. M. E. Gnegy, H. Khoshbouei, K. A. Berg, J. A. Javitch, W. P. Clarke, M. Zhang, A. Galli, Intracellular Ca^{2+} regulates amphetamine-induced dopamine efflux and currents mediated by the human dopamine transporter. *Mol. Pharmacol.* **66**, 137–143 (2004).
38. Y.-J. Yu, C.-H. Huang, C.-H. Chang, P.-W. Gean, Involvement of protein phosphatases in the destabilization of methamphetamine-associated contextual memory. *Learn. Mem.* **23**, 486–493 (2016).
39. A. Kiss, F. Erdődi, B. Lontay, Myosin phosphatase: Unexpected functions of a long-known enzyme. *Biochim. Biophys. Acta Mol. Cell Res.* **1866**, 2–15 (2019).
40. Y. H. Son, J. S. Song, S. H. Kim, J. Kim, Pharmacokinetic characterization of CK2 inhibitor CX-4945. *Arch. Pharm. Res.* **36**, 840–845 (2013).
41. M. H. Cheng, E. Block, F. Hu, M. C. Cobanoglu, A. Sorkin, I. Bahar, Insights into the modulation of dopamine transporter function by amphetamine, orphenadrine and cocaine binding. *Front. Neurol.* **6**, 134 (2015).
42. D. E. Kim, D. Chivian, D. Baker, Protein structure prediction and analysis using the Robetta server. *Nucleic Acids Res.* **32**, W526–W531 (2004).
43. D. Kozakov, D. R. Hall, B. Xia, K. A. Porter, D. Padhorny, C. Yueh, D. Beglov, S. Vajda, The ClusPro web server for protein-protein docking. *Nat. Protoc.* **12**, 255–278 (2017).
44. M. H. Cheng, L. Ponzoni, T. Sorkina, J. Y. Lee, S. Zhang, A. Sorkin, I. Bahar, Trimerization of dopamine transporter triggered by AIM-100 binding: Molecular mechanism and effect of mutations. *Neuropharmacology* **161**, 107676 (2019).
45. G. Khelashvili, A. Galli, H. Weinstein, Phosphatidylinositol 4,5-biphosphate (PIP_2) lipids regulate the phosphorylation of syntaxin N-terminus by modulating both its position and local structure. *Biochemistry* **51**, 7685–7698 (2012).
46. I. Silbern, K.-T. Pan, M. Fiosins, S. Bonn, S. O. Rizzoli, E. F. Fornasiero, H. Urlaub, R. Jahn, Protein phosphorylation in depolarized synaptosomes: Dissecting primary effects of calcium from synaptic vesicle cycling. *Mol. Cell. Proteomics* **20**, 100061 (2021).
47. E. Bowton, C. Saunders, K. Erreger, D. Sakrikar, H. J. Matthies, N. Sen, T. Jessen, R. J. Colbran, M. G. Caron, J. A. Javitch, R. D. Blakely, A. Galli, Dysregulation of dopamine transporters via dopamine D2 autoreceptors triggers anomalous dopamine efflux associated with attention-deficit hyperactivity disorder. *J. Neurosci.* **30**, 6048–6057 (2010).
48. M. S. Mazei-Robison, E. Bowton, M. Holy, M. Schmudermaier, M. Freissmuth, H. H. Sitte, A. Galli, R. D. Blakely, Anomalous dopamine release associated with a human dopamine transporter coding variant. *J. Neurosci.* **28**, 7040–7046 (2008).
49. P. J. Hamilton, N. G. Campbell, S. Sharma, K. Erreger, F. H. Hansen, C. Saunders, A. N. Belovich; NIH ARRA Autism Sequencing Consortium, M. A. Sahai, E. H. Cook, U. Gether, H. S. M. Haourab, H. J. G. Matthies, J. S. Sutcliffe, A. Galli, De novo mutation in the dopamine transporter gene associates dopamine dysfunction with autism spectrum disorder. *Mol. Psychiatry* **18**, 1315–1323 (2013).
50. M. H. Cheng, I. Bahar, Monoamine transporters: Structure, intrinsic dynamics and allosteric regulation. *Nat. Struct. Mol. Biol.* **26**, 545–556 (2019).
51. S. Yamamoto, E. S. Seto, Dopamine dynamics and signaling in *Drosophila*: An overview of genes, drugs and behavioral paradigms. *Exp. Anim.* **63**, 107–119 (2014).
52. T. J. Philyaw, A. Rothenfluh, I. Titos, The use of *Drosophila* to understand psychostimulant responses. *Biomedicine* **10**, 119 (2022).
53. K. Kume, S. Kume, S. K. Park, J. Hirsh, F. R. Jackson, Dopamine is a regulator of arousal in the fruit fly. *J. Neurosci.* **25**, 7377–7384 (2005).
54. J. I. Aguilar, M. H. Cheng, J. Font, A. C. Schwartz, K. Ledwitch, A. Duran, S. J. Mabry, A. N. Belovich, Y. Zhu, A. M. Carter, L. Shi, M. A. Kurian, C. Fenollar-Ferrer, J. Meiler, R. M. Ryan, H. S. Mchaourab, I. Bahar, H. J. G. Matthies, A. Galli, Psychomotor impairments and therapeutic implications revealed by a mutation associated with infantile Parkinsonism-Dystonia. *eLife* **10**, e68039 (2021).
55. Z. Mao, R. L. Davis, Eight different types of dopaminergic neurons innervate the *Drosophila* mushroom body neuropil: Anatomical and physiological heterogeneity. *Front. Neural. Circuits* **3**, 5 (2009).
56. A. Claridge-Chang, R. D. Roorda, E. Vrontou, L. Sjulson, H. Li, J. Hirsh, G. Miesenböck, Writing memories with light-addressable reinforcement circuitry. *Cell* **139**, 405–415 (2009).
57. R. G. Pendleton, A. Rasheed, T. Sardina, T. Tully, R. Hillman, Effects of tyrosine hydroxylase mutants on locomotor activity in Drosophila: A study in functional genomics. *Behav. Genet.* **32**, 89–94 (2002).
58. B. Giros, M. Jaber, S. R. Jones, R. M. Wightman, M. G. Caron, Hyperlocomotion and indifference to cocaine and amphetamine in mice lacking the dopamine transporter. *Nature* **379**, 606–612 (1996).
59. K. Keleman, E. Vrontou, S. Krüttner, J. Y. Yu, A. Kurtovic-Kozaric, B. J. Dickson, Dopamine neurons modulate pheromone responses in *Drosophila* courtship learning. *Nature* **489**, 145–149 (2012).
60. S. X. Zhang, D. Rogulja, M. A. Crickmore, Dopaminergic circuitry underlying mating drive. *Neuron* **91**, 168–181 (2016).
61. R. Andretic, B. van Swinderen, R. J. Greenspan, Dopaminergic modulation of arousal in *Drosophila*. *Curr. Biol.* **15**, 1165–1175 (2005).
62. S. X. Zhang, L. E. Miner, C. L. Boutros, D. Rogulja, M. A. Crickmore, Motivation, perception, and chance converge to make a binary decision. *Neuron* **99**, 376–88.e6 (2018).
63. K. M. Scaplen, K. R. Kaun, Reward from bugs to bipeds: A comparative approach to understanding how reward circuits function. *J. Neurogenet.* **30**, 133–148 (2016).
64. M. Kanno, S. Hiramatsu, S. Kondo, H. Tanimoto, T. Ichinose, Voluntary intake of psychoactive substances is regulated by the dopamine receptor Dop1R1 in *Drosophila*. *Sci. Rep.* **11**, 3432 (2021).
65. K. Nakamura, Y. Iwata, A. Anitha, T. Miyachi, T. Toyota, S. Yamada, M. Tsujii, K. J. Tsuchiya, Y. Iwayama, K. Yamada, E. Hattori, H. Matsuzaki, K. Matsumoto, K. Suzuki, S. Suda, K. Takebayashi, N. Takei, H. Ichikawa, T. Sugiyama, T. Yoshikawa, N. Mori, Replication study of Japanese cohorts supports the role of STX1A in autism susceptibility. *Prog. Neuropsychopharmacol. Biol. Psychiatry* **35**, 454–458 (2011).
66. T. Kofuji, Y. Hayashi, T. Fujiwara, M. Sanada, M. Tamaru, K. Akagawa, A part of patients with autism spectrum disorder has haploidy of HPC-1/syntaxin1A gene that possibly causes behavioral disturbance as in experimentally gene ablated mice. *Neurosci. Lett.* **644**, 5–9 (2017).
67. A. H. C. Wong, J. Trakalo, O. Likhodi, M. Yusuf, A. Macedo, M.-H. Azevedo, T. Klempan, M. T. Pato, W. G. Honer, C. N. Pato, H. H. M. Van Tol, J. L. Kennedy, Association between schizophrenia and the syntaxin 1A gene. *Biol. Psychiatry* **56**, 24–29 (2004).
68. M. A. Castillo Wong, S. Ghose, C. A. Tamminga, P. G. Ulery-Reynolds, Deficits in syntaxin 1 phosphorylation in schizophrenia prefrontal cortex. *Biol. Psychiatry* **67**, 208–216 (2010).
69. S. K. Bhardwaj, C. M. Cassidy, L. K. Srivastava, Changes in syntaxin-1B mRNA in the nucleus accumbens of amphetamine-sensitized rats. *Int. J. Neuropsychopharmacol.* **9**, 751–759 (2006).
70. A. Siddiqui-Jain, D. Drygin, N. Streiner, P. Chua, F. Pierre, S. E. O'Brien, J. Bliesath, M. Omori, N. Huser, C. Ho, C. Proffitt, M. K. Schwaebe, D. M. Ryckman, W. G. Rice, K. Anderes, CX-4945, an orally bioavailable selective inhibitor of protein kinase CK2, inhibits prosurvival and angiogenic signaling and exhibits antitumor efficacy. *Cancer Res.* **70**, 10288–10298 (2010).
71. H. Soehnge, X. Huang, M. Becker, P. Whitley, D. Conover, M. Stern, A neurotransmitter transporter encoded by the Drosophila inebriated gene. *Proc. Natl. Acad. Sci. U.S.A.* **93**, 13262–13267 (1996).
72. A. Sanz-Clemente, J. A. Gray, K. A. Ogilvie, R. A. Nicoll, K. W. Roche, Activated CaMKII couples GluN2B and casein kinase 2 to control synaptic NMDA receptors. *Cell Rep.* **3**, 607–614 (2013).
73. C. Saunders, J. V. Ferrer, L. Shi, J. Chen, G. Merrill, M. E. Lamb, L. M. F. Leeb-Lundberg, L. Carvelli, J. A. Javitch, A. Galli, Amphetamine-induced loss of human dopamine transporter activity: An internalization-dependent and cocaine-sensitive mechanism. *Proc. Natl. Acad. Sci. U.S.A.* **97**, 6850–6855 (2000).
74. K. M. Kahlig, J. A. Javitch, A. Galli, Amphetamine regulation of dopamine transport. Combined measurements of transporter currents and transporter imaging support the endocytosis of an active carrier. *J. Biol. Chem.* **279**, 8966–8975 (2004).
75. K. M. Kahlig, B. J. Lute, Y. Wei, C. J. Loland, U. Gether, J. A. Javitch, A. Galli, Regulation of dopamine transporter trafficking by intracellular amphetamine. *Mol. Pharmacol.* **70**, 542–548 (2006).
76. G. E. DiCarlo, J. I. Aguilar, H. J. G. Matthies, F. E. Harrison, K. E. Bundschuh, A. West, P. Hashemi, F. Herborg, M. Rickhag, H. Chen, U. Gether, M. T. Wallace, A. Galli, Autism-linked dopamine transporter mutation alters striatal dopamine neurotransmission and dopamine-dependent behaviors. *J. Clin. Invest.* **129**, 3407–3419 (2019).
77. K. M. Kahlig, F. Binda, H. Khoshbouei, R. D. Blakely, D. G. McMahon, J. A. Javitch, A. Galli, Amphetamine induces dopamine efflux through a dopamine transporter channel. *Proc. Natl. Acad. Sci. U.S.A.* **102**, 3495–3500 (2005).
78. L. Carvelli, R. D. Blakely, L. J. DeFelice, Dopamine transporter/syntaxin 1A interactions regulate transporter channel activity and dopaminergic synaptic transmission. *Proc. Natl. Acad. Sci. U.S.A.* **105**, 14192–14197 (2008).
79. D. G. Fisher, G. L. Reynolds, L. E. Napper, Use of crystal methamphetamine, Viagra, and sexual behavior. *Curr. Opin. Infect. Dis.* **23**, 53–56 (2010).
80. M. Dubol, C. Trichard, C. Leroy, A. L. Sandu, M. Rahim, B. Granger, E. T. Tzavara, L. Karila, J.-L. Martinot, E. Artiges, Dopamine transporter and reward anticipation in a dimensional perspective: A multimodal brain imaging study. *Neuropsychopharmacology* **43**, 820–827 (2018).
81. G. F. Koob, N. D. Volkow, Neurobiology of addiction: A neurocircuitry analysis. *Lancet Psychiatry* **3**, 760–773 (2016).

82. F. Pierre, P. C. Chua, S. E. O'Brien, A. Siddiqui-Jain, P. Bourbon, M. Haddach, J. Michaux, J. Nagasawa, M. K. Schwaebe, E. Stefan, A. Vialettes, J. P. Whitten, T. K. Chen, L. Darjania, R. Stansfield, K. Anderes, J. Bliesath, D. Drygin, C. Ho, M. Omori, C. Proffitt, N. Streiner, K. Trent, W. G. Rice, D. M. Ryckman, Discovery and SAR of 5-(3-Chlorophenylamino)benzo[c][2,6]naphthyridine-8-carboxylic Acid (CX-4945), the first clinical stage inhibitor of protein kinase CK2 for the treatment of cancer. *Med. Chem.* **54**, 635–654 (2011).
83. K. N. Colbert, D. A. Hattendorf, T. M. Weiss, P. Burkhardt, D. Fasshauer, W. I. Weis, Syntaxin1a variants lacking an N-peptide or bearing the LE mutation bind to Munc18a in a closed conformation. *Proc. Natl. Acad. Sci. U.S.A.* **110**, 12637–12642 (2013).
84. J. E. Dowling, C. Chuaqui, T. W. Pontz, P. D. Lyne, N. A. Larsen, M. H. Block, H. Chen, N. Su, A. Wu, D. Russell, H. Pollard, J. W. Lee, B. Peng, K. Thakur, Q. Ye, T. Zhang, P. Brassil, V. Racicot, L. Bao, C. R. Denz, E. Cooke, Potent and selective inhibitors of CK2 kinase identified through structure-guided hybridization. *ACS Med. Chem. Lett.* **3**, 278–283 (2012).
85. E. L. Wu, X. Cheng, S. Jo, H. Rui, K. C. Song, E. M. Dávila-Contreras, Y. Qi, J. Lee, V. Monje-Galvan, R. M. Venable, J. B. Klauda, W. Im, CHARMM-GUI membrane builder toward realistic biological membrane simulations. *J. Comput. Chem.* **35**, 1997–2004 (2014).
86. J. C. Phillips, R. Braun, W. Wang, J. Gumbart, E. Tajkhorshid, E. Villa, C. Chipot, R. D. Skeel, L. Kalé, K. Schulten, Scalable molecular dynamics with NAMD. *J. Comput. Chem.* **26**, 1781–1802 (2005).
87. W. Humphrey, A. Dalke, K. Schulten, VMD: Visual molecular dynamics. *J. Mol. Graph.* **14**, 33–38 (1996).

Acknowledgments: We would like to acknowledge Saunders Consulting for the help in editing this manuscript. **Funding:** This study was supported by the National Institute of Drug Abuse grant RO1DA038058 (A.G. and H.J.G.M.) and RO1DA035263 (A.G. and H.J.G.M.). **Author contributions:** Conceptualization: A.S., S.J.M., I.B., A.M.C., H.J.G.M., and A.G. Investigation: A.S., S.J.M., M.H.C., J.I.A., S.P., D.Z., D.P.S., Y.Z., T.R., and H.J.G.M. Visualization: A.S., S.J.M., M.H.C., and J.I.A. Supervision: A.M.C., I.B., H.J.G.M., and A.G. Writing—original draft: A.S., S.J.M., A.M.C., and A.G. Writing—review and editing: A.S., S.J.M., M.H.C., P.U.-R., I.B., A.M.C., H.J.G.M., and A.G. **Competing interests:** The authors declare that they have no competing interests. **Data and materials availability:** All data needed to evaluate the conclusions in the paper are present in the paper and/or Supplementary Materials. All parameter files used in the modeling, the codes for running NAMD, and the initial ClusPro-predicted hDAT-Stx1 complex model are provided in the Supplementary Materials.

Submitted 7 July 2022
Accepted 14 December 2022
Published 11 January 2023
10.1126/sciadv.add8417